# SEARCH FOR NEW PHENOMENA IN LOW-MASS DIJET USING TRIGGER-LEVEL ANALYSIS

HERJUNO NINDHITO

THESIS SUBMITTED FOR THE DEGREE OF MASTER OF SCIENCE

SUPERVISED BY CATERINA DOGLIONI

DEPARTMENT OF PHYSICS– FACULTY OF SCIENCE

MAY 2016


LUND UNIVERSITY

*"Only death can finish the fight, everything else only interrupts the fighting."*

— Andrzej Sapkowski

*"We are an impossibility in an impossible universe."*

— Ray Bradbury

## ABSTRACT

The recent upgrade of the Large Hadron Collider (LHC) benefits searches for new physics phenomena using multijet final states. The increased center-of-mass energy opens new possibilities to probe new physics at scales beyond the Tera-electron volt (TeV), especially in di-jet final states. However, in the sub-TeV mass region, the QCD background to dijet searches is overwhelming and not all events can be fully recorded. Due to the limited bandwidth available for offline storage, the rates of recording events have to be kept under control. This bandwidth limitation could be addressed by recording partial events, reducing the event size drastically. In order to use these partial events, recorded within the High Level Trigger (HLT) system in a search for new physics, a new dedicated calibration scheme needs to be developed. This thesis describes the data-driven in-situ pseudorapidity ($\eta$) intercalibration for HLT jets that is necessary for such a search.

*"What I am going to tell you about is what we teach our physics students in the third or fourth year of graduate school... It is my task to convince you not to turn away because you don't understand it. You see my physics students don't understand it... That is because I don't understand it. Nobody does."*

— Richard Feynman [1]

## ACKNOWLEDGMENTS

There are so many people that I would like to acknowledge for what they have done.

First of all, I would like to thank my parents and my family, especially my mother for allowing me to go this far, literally and figuratively. Both of you never questioned my choice even for just a single bit. I am truly grateful for all of your support.

For my supervisor, Caterina Doglioni, I would never ever be able to thank you enough. You showed me not only how to be a good scientist, but also how to be a better person in life. You were teaching with example and never afraid of getting your hands dirty. Your love and passion for particle physics are nothing but admirable. I am still amazed by how much you put your trust on me after all this time. Torsten definitely made a great decision to bring you here, Lund is better with you on board.

I also want to send my gratitude to Torsten Åkesson. He is one of the wisest man I have ever met. Whenever he speaks, everyone is just stop and listen. I would also say thanks for Oxana for her teaching and for being a fierce competitor on "the last man standing in the office". Another division member that I want to say thanks: Balasz for the amazing guide of Hungary and a brief history of Europe, Florido the party master, and Else for all the ATLAS' nominations :p. I would like also say thanks to Anders Oskarsson for his help during my first year.

Thanks to the awesome TLA team: Antonio, Caterina(again), Guy, Kate, Merlin, and Frederik. I really enjoy working with you guys. To Jacob and Michaela, this thesis would never materialized without your awesome intercalibration package. Many thanks to Andy Pilkington and Steven Schramm for always telling me that my result is important, even though I had no idea at that time.

Prim. Primrose "patrawan" Everdeen. I would never have a partner in crime better than you. We came from the same place, going through a lot of stuff together, and ended up working with Caterina also together. You always make me feels like home. Many thanks to Connor with extra n as well. I hope you enjoy your time in Warwick. For my other office mates: Nicholai, Rickard, Sebastian, and Vilhelm, thanks for the heart-warming discussions on and off physics.

My thesis was also supported by Lund's phd students: Edgar, Trine, Sasha, Lene, Vytautas, Martin, Tuva, Ben, and of course Anders the board game master. I wish you guys all the success in the future!

To my friends since the beginning of my time in Lund: Morten, Brian, Madeleine, Benjamin, Jim, and Fredrik, thanks for helping me adapting to life in this far-far away place. I hope someday we can see each other again. I would also like to send my gratitude to the guy that I considered as my own brother: Jirka Mnuk. You taught me a lot of things in life, especially on how to live in European way.

I want to send a special thanks for Justin and Dan Hawkins, Frankie Poullain, Rufus Taylor, and Emily Davies of The Darkness for producing and performing such

remarkable music in the Last of Our Kind. #therealjustin is only one and it is Justin Dawkins!

For my Indonesian fellows, thanks for keeping my ability to speak Bahasa in check. In particular, thanks to Monica for the invaluable weekly food and always being a great partner in discussion. I owe you a lot of stuff, literally and figuratively.

This thesis was funded by Indonesian Endowment Fund for Education. I'll bring particle physics back home someday.

# SELF REFLECTION

When I reflect on these past two years, I still cannot believe how far I have been walking. At the point when I decided to be a particle physicist, I never thought that it is going to be this way.

A sudden change from applied physics to fundamental physics is never easy. However, from my bumpy first year, I realized that our universe is such a beautiful puzzle that awaits to be solved. I also knew the steep learning curve that I need to overcome in the future as my pursuit of an answer for that puzzle. In the world full of talented and extraordinary people, I can only do nothing but work hard. There is a small odd, as little as Leicester City's odd to win the Premier League in 2015, that I can survive in physics. Guess what? I always love beating the odds.

My luck began to change when I started this thesis. I met Caterina and went to CERN straight away. It felt amazing, almost like a kid in a Willy Wonka's factory. Starting from presenting a plot in the third day I am learning ROOT, I learned that I need to work as fast and efficient as possible. Many things can escalate pretty quickly, trust me.

Throughout the first half of my thesis, I familiarized myself with the ROOT, Python, and C++. Much hard-coding and self-taught at the first time, but I am getting better at it now. After all, being a good particle physicist is equal to being a good programmer.

I also started to get involved more in the ATLAS meetings and was lucky enough to be part of the Trigger Level Analysis team. Working in a team is not a small feat, but I always try not to let down my teammates. I failed in many occasions, but I keep on learning to be a good team player.

In January 2016, I started to work on the eta intercalibration for HLT jets. Caterina gave me a complete freedom on how to address this matter. I learnt to work in more independent way and put all of my knowledge into practice. It was fun! Shortly after that, I had a chance to make my result into a public plot. Luckily, TLA team was also in the process of making a conference note, so I was involved in the process since the very beginning.

This thesis teaches me a lot of things. Not only the physics aspect of it but also about how to be a good team player and other things that I needed for my future career. I'm really grateful for it.

It was a joyful ride! Thanks for everyone who are being a part of it.

## POPULAR SCIENCE

Ever since the beginning of time, our understanding of the universe is always driven by our curiosity. By questioning about natural phenomenon around us, we started to investigate the mechanism behind them. Those phenomenon turns out to work on some sort of patterns. The idea that those patterns are part of a bigger picture of a natural order was out of the question at that time. However, once we understood the trivial things around us, a new set of questions emerge: Where do we come from? How our universe was made? What are the most fundamental blocks in the universe?

The Large Hadron Collider (LHC) at CERN is one of the experiments built to answer those questions. LHC is built as 27-kilometers-circumference circular collider who is ready to collide protons or lead ions to mimic the condition of the very first second of our universe. Through ATLAS, one of the LHC's detector, physicists try to capture the particles that produced from the collisions. It is achieved by colliding bunches of protons at nearly the speed of light, with an energy up to 13 tera electronvolts (TeV). One TeV is equal to $10^{12}$ electronvolts. An electronvolt is an unit of energy that is needed to accelerate electron through one volt of potential difference. To put that into perspective, 13 TeV is about the energy of 13 flying mosquitoes, but packed in a space trillions times smaller than mosquito. These amount of energies has never been reached in a laboratory before, making it possible to discover new phenomena that were previously inaccessible.

LHC had successfully observed the Higgs boson in 2012. Finding this particle was necessary for our understanding of nature, but it is predicted by physicists. The Higgs boson completes the Standard Model (SM) theory, a basic theory that explain fundamental interactions between sub-atomic particles. Unfortunately, it does not help physicists explaining the existence of unknown phenomena like dark matter (DM). Dark matter is an unknown matter which fill roughly a quarter of our universe. As a comparison, the usual visible matter (stars, planets, etc) only accounts for 5% out of the universe's content. Many theorists expect dark matter to interact with the visible matter, to explain its abundance in the present universe.

To understand the nature of dark matter, physicists are exploiting experimentally observed objects called *jet*. Jet is a bunch of collimated high energy deposits in a detector, resulting from the collisions at the LHC. The interaction between SM and DM particles can be mediated by a new mediator particle which can decay into jets.

In order for a physics model with a DM mediator to be consistent with the observed DM abundance in the universe, a mediator must have a mass below 1 TeV. However, probing this region is as difficult as finding needle in a haystack. There are tons of known particles, called *backgrounds*, which produced much more often than the rare DM mediator particle decay.

In order to distinguish a rare event from the rest of the collision, a collision event should have at least two jets in a back-to-back direction between one and another. Then, an event is selected based on their energy, to remove low-energy processes that dominate the backgrounds.

Even though those selections have reduced the event rates significantly, there are still too many events to record. One of the solutions to this problem is by applying

a prescaling which selects an event for every-n occurrences. However, it is clear that prescaling will also randomly discard rare events that we are looking for.

To avoid this limitation, physicists reduce the information that is being recorded from a collision event, so that it has smaller size. As a consequence, more events can be recorded without the need for prescaling! Due to its limited information, these events will be partially-reconstructed into physics objects for further analysis. However, a set of dedicated jet calibration needs to be applied to bring it as close as possible to the fully reconstructed events which has a full information in it. Such correction is first derived from a Monte Carlo (MC) event simulation. The detector dependent effects that cannot be corrected by simulation are corrected via a data-driven calibration that accounts for the discrepancy because of the detector geometry. This calibration is derived in this thesis, and the result now show a good agreement between partial and full-event reconstruction.

By exploring this data-driven correction in the future research, a search in the sub-TeV mass region is looking as bright as it ever been. With the upcoming 2016 data taking, one could expect more exciting result ahead.

# CONTENTS


1 INTRODUCTION 1
1.1 A new frontier in the sub-TeV mass region . . . 1
1.2 Thesis outline . . . 1
1.3 Author's contribution . . . 2
2 THEORETICAL BACKGROUND 3
2.1 Standard Model Physics . . . 3
2.2 Quantum Chromodynamics and jets . . . 4
2.2.1 Quarks as nucleon's sub-structure . . . 4
2.2.2 Asymptotic freedom and quark confinement . . . 5
2.2.3 Jets and LHC . . . 6
2.3 Monte Carlo event generator . . . 7
2.4 New phenomena of physics beyond standard model . . . 7
3 THE ATLAS EXPERIMENT 10
3.1 Challenge and physics potential for jet-based analysis of LHC Run-2 . . . 10
3.2 ATLAS detector . . . 12
3.2.1 Coordinate system . . . 13
3.2.2 ATLAS calorimeter . . . 13
3.3 Jet reconstruction . . . 17
3.4 Run-2 ATLAS TDAQ system . . . 17
3.4.1 Run-2 trigger system . . . 18
3.4.2 Data acquisition system . . . 19
3.5 Data processing in ATLAS . . . 21
4 TRIGGER LEVEL ANALYSIS 23
4.1 Triggering strategy for TLA . . . 23
4.2 Jet energy calibration . . . 23
4.2.1 Pile-up correction . . . 25
4.2.2 Jet energy scale correction . . . 26
4.2.3 Residual in-situ correction . . . 26
4.2.4 Eta inter-calibration . . . 28
4.3 Jet energy scale validation . . . 29
5 RESULT AND DISCUSSION 31
5.1 Event selection . . . 31
5.1.1 Real data . . . 31
5.1.2 Simulated data . . . 31
5.1.3 TLA selection . . . 32
5.2 Eta intercalibration result . . . 32
5.2.1 Eta binning . . . 32
5.2.2 Comparison of $\eta$ inter-calibration method . . . 33
5.2.3 Comparison of data with MC . . . 34
5.2.4 Trigger and offline jet comparison . . . 35
5.3 Validation with multijet events . . . 36
6 SUMMARY 37
A APPENDIX 38
A.1 Comparison of data with MC . . . 38

A.2 Trigger and offline jet comparison . . . . . 44

BIBLIOGRAPHY 50

# 1 INTRODUCTION

## 1.1 A NEW FRONTIER IN THE SUB-TEV MASS REGION

Particle physics as a branch of physics that studies the phenomena in the sub-atomic scale is recently entering an exciting era. A new 13 TeV energy regime with much higher collision rates opens more possibilities for searches of the new physics. Those new developments are important because the discovery of Higgs boson in 2012 leaves more questions on the Standard Model (SM) theory, especially on its relationship with the unexplained phenomena such as the dark matter (DM). How DM particle interact with SM particles remains as an open question.

The SM theory predicts the existence of sub-atomic interactions with a remarkable degree of precision. Its predictive power has aided the development of increasingly bigger accelerators in order to investigate the most fundamental component of matter. Stanford Linear Accelerator (SLAC), Tevatron, and Large Hadron Collider (LHC) are few examples of accelerators that have been constructed with discovery in mind. LHC, however, is the only collider left to date with high enough energy to perform TeV scale search of the new physics beyond standard model (BSM).

The high collision energy provided by the LHC is able to break innermost structure of the colliding particles and reveal its contents. The released energy then materialized as new particles. It will further decay into much more stable particles which could be detected by the LHC's detectors.

The search for DM resonance via dijet final states is one of the frontrunner DM search during the Run-2 LHC data taking[2]. One of the simplest models involves an additional mediator particle which couples with the standard model particles[3].

Modern colliders with ever-increasing available energies favour high-mass searches due to the availability of the additional mass regions that can be explored. Many searches were performed at energies above 1 TeV[4] without finding any new physics. Sub-TeV searches were often overlooked and uncovered because of the overwhelming QCD background that makes it impossible to record all events. This region is important because the dark matter mediator might have masses below 1 TeV. Therefore, a new method to explore this region is needed.

The *Data scouting* (DS) method pioneered by the CMS collaboration was then implemented in the ATLAS experiment. Data scouting stream only records a fraction of information, reducing the event size to a bare minimum to perform simple event reconstruction. The resulting objects do not in principle have the same performance as the fully reconstructed ones. However, a partially reconstructed object could match the fully reconstructed one by choosing a suitable calibration strategy.

This thesis will focus on data-driven calibration procedures for the partially reconstructed jets, where the fully reconstructed jets act as a standard for comparison.

## 1.2 THESIS OUTLINE

After a short introduction, a brief theoretical background will be presented in Chapter 2. Some fundamental aspects of jet physics are covered to give a foothold for inter-

preting the experimental result. Then the technical side of the experiment will follow in Chapter 3. The analysis strategy for *Trigger level analysis*(TLA) and the result will be presented in Chapter 4 and Chapter 5. Lastly, a quick summary will be given in Chapter 6.

## 1.3 AUTHOR'S CONTRIBUTION

The ATLAS experiment is a large experimental collaboration with more than 5000 scientists from around the world. All of its publications are made under the name of the collaboration. To be eligible as an author, one needs to work on a qualification task, usually during their first year of Ph.D. However, being part of an analysis team and contribute to the work of the analysis is still possible.

During my time as a master student in ATLAS, I was involved in the Trigger-Level Analysis (TLA) team. I was mainly responsible for deriving a dedicated pseudorapidity ($\eta$) inter-calibration for trigger jets 4.2.4, and validating the calibration procedure using the Multi-jet balance technique. I was able to prepare reference trigger rate plots of data scouting stream on 13 TeV data [5] and eta inter-calibration plot for trigger jets [6]. I am also involved in data scouting jet plots [7].

# 2

# THEORETICAL BACKGROUND

This chapter describes the underlying motivations for this thesis from the theoretical point of view. Section 2.1 gives a brief summary of the Standard Model (SM) physics. In 2.2, some important aspects of QCD and jet physics are given. A quick introduction on a Monte Carlo (MC) event generator follows in 2.3. Finally, section 2.4 deals with the new phenomena beyond the Standard Model (BSM).

## 2.1 STANDARD MODEL PHYSICS

The Standard Model is a theory which explains our current understanding of fundamental particles and their interactions. It describes the basic building blocks of the matter called *fermions* and the mediators of interactions called *bosons*. There are twelve fermions and five bosons discovered as shown in Figure 1. Three out of the four

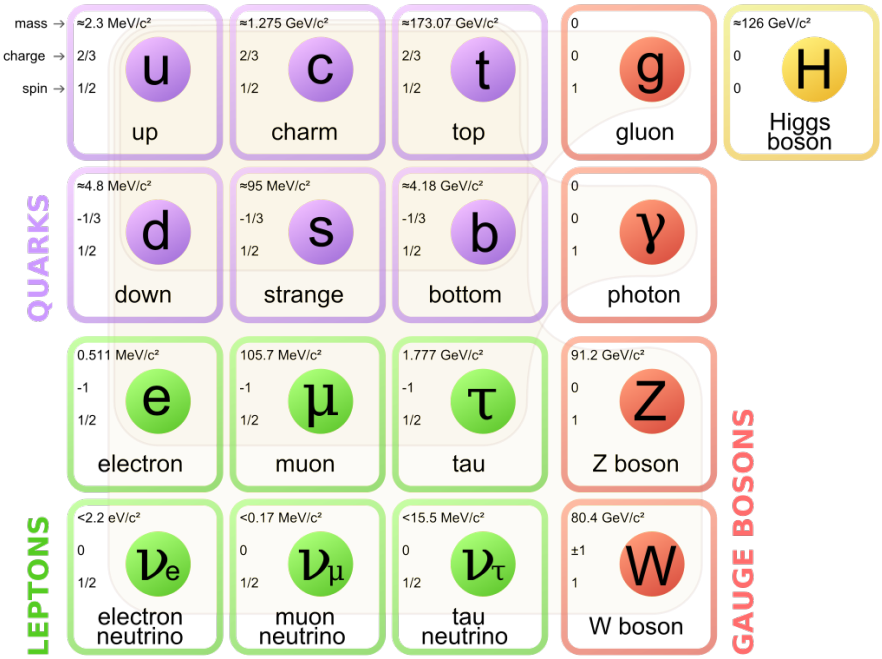


Figure 1: Particles the in the standard model theory. Three generation of quarks and Leptons are shown with the bosons in fourth and fifth column.

fundamentals forces are included in the Standard Model: the electromagnetic, strong, and weak forces. Electromagnetism is carried by photons and affects both quarks and charged leptons, while intermediate vector bosons, such as $W^{\pm}$ and Z, are the carriers of the weak force. Unlike the electromagnetic force, the weak force affects all quarks and leptons. On the other hand, the strong force comes into play via gluons where only quarks are affected. Gravity has not yet been explained and integrated into the SM. A *graviton* as gravity's mediator remains elusive to date. Table 1 shows that gravity is too weak to give any notable effect on our particle interactions.

| FORCE | RELATIVE STRENGTH | RANGE OF INTERACTIONS |
|---|---|---|
| EM | 1/138 | $\infty$ |
| Weak | $10^{-6}$ | $10^{-18}$ |
| Strong | 1 | $10^{-15}$ |
| Gravity | $10^{-39}$ | $\infty$ |

Table 1: Four fundamental forces in the universe with its range of interaction and respective strength relative to the strong force

Even though the discovery of the Higgs boson is regarded as a milestone in the completion of the SM theory, there are more issues which remain unexplained. The exclusion of gravity, the non-zero mass of the neutrinos, and the proof of existence of the dark matter from cosmological observations give strong motivations on further searches for the new physics beyond Standard Model.

## 2.2 QUANTUM CHROMODYNAMICS AND JETS

### 2.2.1 *Quarks as nucleon's sub-structure*

Quantum chromodynamics (QCD) is a theory which describes the nature of strong interactions. The idea of compositeness of a hadronic state started from the pion discovery in 1947 by Powell[8]. His experiment concludes that the elastic nucleon form factors, both electric and magnetic, are falling off rapidly along with the momentum transfer. This discovery implies that the pions were produced with a direction almost collinear with the beam axis, instead of filling all the available phase space. In other words, if the proton is hit with enough energy, it will be more likely to break into smaller, more fundamental pieces.

To test this idea, a collaboration between SLAC and MIT built a high energy electron-proton experiment to investigate a deep-inelastic scattering. The concept was similar to the Rutherford's atomic nucleus experiment but with much higher energies. The SLAC-MIT experiment used a 20 GeV electron beam made to hit a static hydrogen target. If proton was a complex and weakly bounded object, the scattering rates should be low. However, the SLAC-MIT team saw a significant rate for electron-proton scattering as if the proton was not an elementary particle. This is because the recoil particles were dominated by numerous hadrons from the deep-inelastic scattering instead of a single proton scatterings.

How could it be possible to have a hard electromagnetic scattering out of nucleon even though there were no hard scattering from the strong interactions? Understanding the kinematics of the deep-inelastic scattering is crucial to answer this question. Figure 2 shows the deep-inelastic scattering process where $k$ and $k'$ denote the four-momenta of the incoming and outgoing electron. $P$ is the four-momenta of a proton with a mass $M$, while $W$ is the mass of the recoiling particles. The cross section can be written in terms of structure functions $F_{1,2}(x, Q^2)$:

$$\frac{d\sigma}{dx dQ^2} = \frac{1}{Q^4}(f_1(y)F_1(x, Q^2) + f_2(y)F_2(x, Q^2)), \tag{1}$$

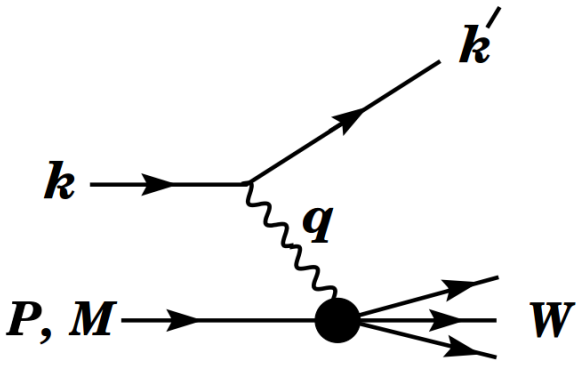


Figure 2: Kinematics of deep-inelastic scattering. A momentum transfer q is carried by $\gamma$ , $W^{\pm}$, or Z. A collection of hadrons is produced with invariant mass W [9].

where x refers to the fraction of proton's momentum transferred to the struck partons, point-like constituents of hadrons (e.g proton), and $Q^2 = -q^2$ are the square of momentum transferred between electron and proton. In general, structure functions are just mathematical functions which are measured experimentally to describe the nucleon behaviour. As a side note, the functions of partons' momentum distribution within the proton are called *Parton Distribution Functions (PDF)*.

The structure functions were then calculated, and the result revealed that they were independent from the momentum transfer. This discovery, called Bjorken scaling, i.e.

$$F_{1,2}(x, Q^2) \to F_{1,2}(x), \tag{2}$$

was entirely different from its elastic counterpart. Bjorken scaling acts as a proof that the interactions inside the proton were point-like. It is also observed that $F_1$ and $F_2$ are satisfying the Callan-Gross relation for particle with spin 1/2:

$$F_2(x) = 2xF_1(x) \tag{3}$$

This point-like, charged particle with spin 1/2, later on, will be known as quark.

### 2.2.2 *Asymptotic freedom and quark confinement*

Bjorken scaling, however, contradicts the fundamental aspect of the Quantum Field Theory (QFT), a theory of quantum mechanics on the fields. In QFT, fermions, like quarks, should interact by exchanging virtual particles which could have large momenta in a small distance inside the nucleon. Since QFT should also apply to that scale, the existence of a free-particle equation is unlikely. Hence, the experimental discovery of almost free quarks and the core principle of QFT did not agree.

The key point to this issue is the fact that the strong interaction has an important feature called *asymptotic freedom*. It means that bonds between quarks are asymptotically weaker with shorter distances and higher energies. This behaviour, therefore, permits high momentum transfer in such short distances and vice versa. Figure 3 shows the evolution of coupling constant $\alpha_s$ along with the incremental growth of the momentum transfer Q.

It is also important to note that no single quark has been observed to date. When one want to separate two quarks into two single quark, one will need enormous energy

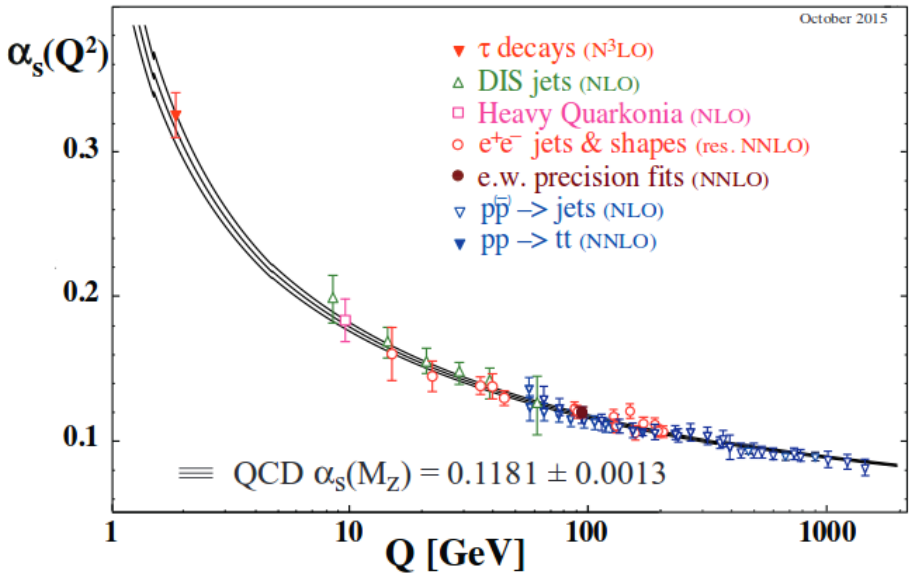


Figure 3: Multiple measurements of the coupling constant $\alpha_s$ as a function of energy Q in GeV.[9]

which in turn produce more quarks. Those quarks then will interact between one and each other into bound states.

However, since quarks are fermions, they should obey the Pauli principle, which is not true even for proton. Proton has two up quarks and one down quark altogether in the same bound state. Therefore, quarks and its mediator, gluons, should carry another property called color charge. Color charge is a conserved quantity as a consequence of QCD's global invariance under SU(3).

### 2.2.3 *Jets and LHC*

The concept of parton is useful not only in describing the initial but also the final state of hadronic collisions. Even though the confinement will prohibit the existence of free partons in the final state, a careful study of the distribution function of the final-state particles will reveal the physics behind the strong interaction in a short distance.

One of the methods to investigate the final-state particles is by using a collection of collimated high-energy objects called *jet*. Jet is reconstructed by a particular algorithm by using detector's inputs. A jet algorithm should be collinear and infrared-safe. A collinear safe algorithm makes sure small-angle splitting does not give any difference in algorithm's performance. On the other hand, infrared-safe requirement will guarantee its ability to retain consistency in the results even after soft QCD emission. The algorithm also needs to have a good performance in presence of detector effects to make it experimentally viable. This thesis will use *anti*-$k_t$ as the primary jet reconstruction algorithm, which will be elaborated more in the Section 3.3.

Figure 4 shows one of the events with the highest jet energy from LHC Run-2. The back-to-back high transverse momentum jets are shown in two green bars that go to two opposite directions, showing the energy deposited in the calorimeters.

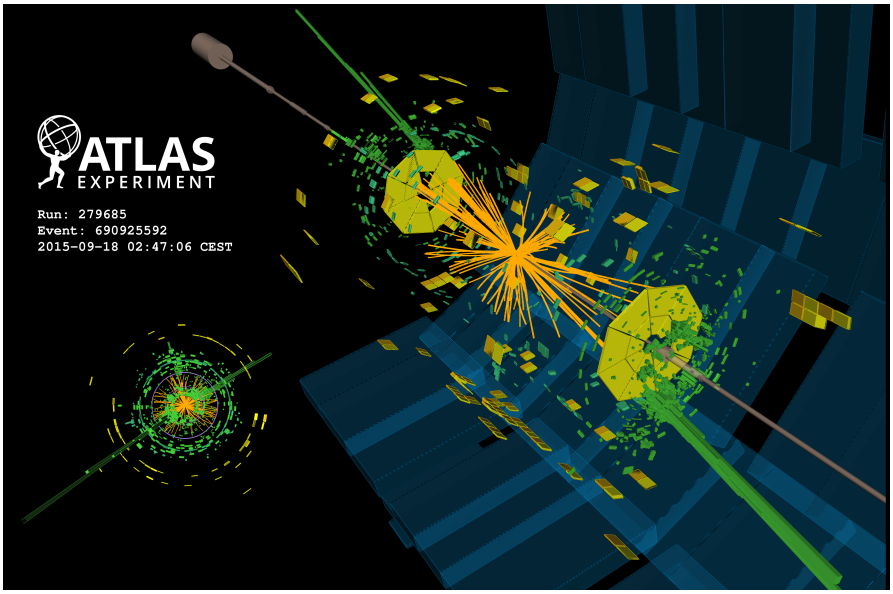


Figure 4: A high-mass dijet event from ATLAS Run-2. The event was taken in September 2015[10].

## 2.3 MONTE CARLO EVENT GENERATOR

Physicists rely heavily on Monte Carlo (MC) software event generators to make a theoretical prediction of the SM and possible deviations from it. The simulation used by modern LHC experiments can calculate finite perturbative expansions of hadronic collisions by using a series of different generators. Figure 5 shows an example of the particle shower from a *p-p* collision that will be simulated by the MC before adding the detector effect. It could be broken down into five phases: *hard process, parton shower, hadronization, underlying event, and particle decay*. The hard scatter happens when two quarks or gluons interact with a large momentum transfer. Lowest order perturbation calculation in the Parton Distribution Function (PDF) gives the probabilistic distributions of the outgoing particles. Then, scattered quarks and gluons are starting to interact between one and another. Soft gluons are the main products of this phase. Parton showers will keep happening until the available momentum is below the perturbation limit. Due to the confinement, quarks will soon cramp together into hadronic bound states. This process often refers as *hadronization*. Some hadrons with long enough decay time will be detected by the detector, as showers of particles interacting in the calorimeters. High energy collisions often leave some remnants which also have enough energy to interact, called an underlying event. Finally, the hadrons will decay further into more stable and lighter particles.

This thesis will use Pythia and Sherpa generated sample as a comparison [12].

## 2.4 NEW PHENOMENA OF PHYSICS BEYOND STANDARD MODEL

While the Higgs discovery in 2012 has completed one of the missing pieces of the SM theory, some questions remain unanswered, such as the integration of gravity into the SM and the search for dark matter. Dark matter remains elusive, but its existence is undeniable from different sources of evidence such as gravitational lensing, velocity curves of spinning galaxies, and cosmic microwave background observation[13].

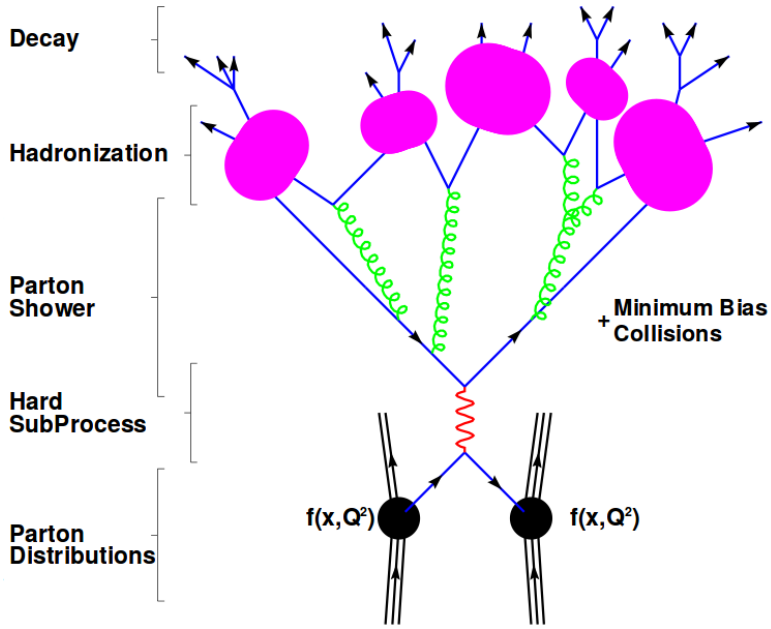


Figure 5: Particle shower process from p-p collision. The decaying particles are the only one that will deposit energy in the calorimeters[11].

Three complementary ways of searches are now being explored: the direct, indirect, and collider based searches[14]. ATLAS, as one of the biggest ground-based detectors to date continues its duty on the collider search.

In contrast to direct and indirect detections that focused on DM-candidate scattering and annihilation, collider search will take a look at a strongly-coupled DM-candidate.

A simplified model for the creation of the dark matter involves an additional mediator particle which couples with SM particles[2]. This mediator further decays into a pair of jets. Figure 6 shows the progress of the constraints on such mediator, called a $Z'$, with coupling $g_B$ [15] from different experiments.

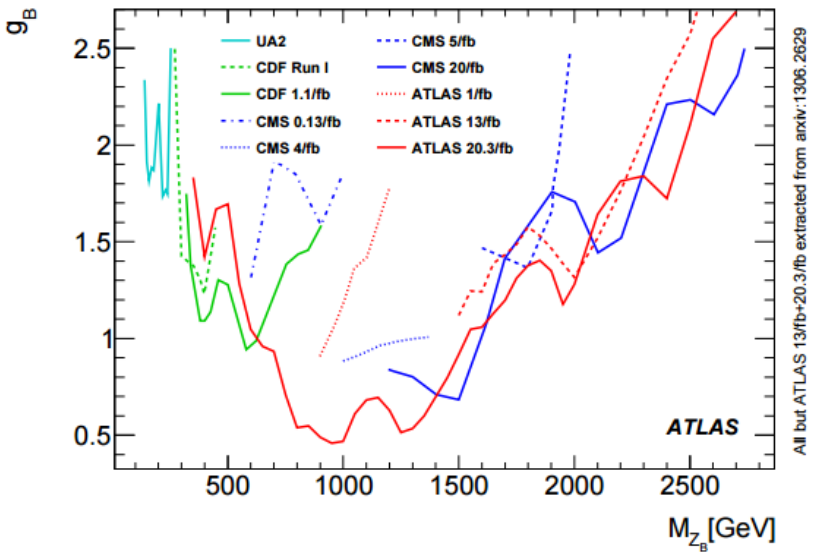


Figure 6: Limit comparison of Z′ resonance from UA2, CDF, CMS, and ATLAS[4].

The lower-mass region is not probed as good as the high-mass because of the enormous QCD background. In this region, signal and background is hard to distinguish because they both produce similar dijet events, such as the WZ productions. The overall event rate is so high that the experiment could not record all events. Along with the rarity of the new physics event sought, this limitation raises a problem: one needs to increase collision rates to make interesting events happen more often, but the events are also getting harder and harder to select. There is a need for a new technique which is able to record events as efficiently as possible. In ATLAS, a new exploration has been made using the *data scouting* and *Trigger Level Analysis (TLA)* technique. This strategy will be described more in the upcoming chapters.

# 3

# THE ATLAS EXPERIMENT

CERN is the European organization for Nuclear Research that operates the biggest particle physics experiments in the world. It is based in Geneva and built with fundamental physics researches in mind. CERN is also the home of the Large Hadron Collider (LHC) with numerous experiments and detectors, such as ATLAS, ALICE, CMS, and LHCb. The LHC lies 100 meters below the ground underneath the Jura mountains. A center-of-mass (CM) collisions energy of 13 TeV is explored in the four interaction points of the LHC, along its 27 km accelerator circumference.

Section 3.1 covers the challenge and physics potential of the newly-upgraded LHC. Next, section 3.2 gives an introduction to the ATLAS detector. An upgrade of trigger and data acquisition system in ATLAS is given in 3.4. Finally, section 3.5 addresses data processing stream in the ATLAS experiment.

## 3.1 CHALLENGE AND PHYSICS POTENTIAL FOR JET-BASED ANALYSIS OF LHC RUN-2

CERN has been built with a continuous improvement in mind. Former accelerators which usually have lower energy, are being used as injectors for bigger accelerators built later on. The Proton Synchrotron (PS) built in 1959 acted as a proton booster for the bigger Super Proton Synchrotron (SPS) when it became operational in 1976. The same thing applied when PS-SPS acted as boosters to the LHC starting from 2010. Figure 7 shows the latest accelerator complex. The LHC itself is also built in several stages of upgrading. In the long shutdown 1 (LS1) period between 2012-2015, the LHC has undergone a major upgrade to make it work with the designed center-of-mass (CM) energy at 13 TeV. It almost doubles the previous peak CM energy in Run-1 at 7-8 TeV. Run-2 also uses a 25 ns bunch spacing, as opposed to the 50 and 75 ns spacing of Run-1, to increase its collision rates [1]. A smaller bunch spacing means higher crossing rate, which will deliver higher beam intensity and luminosity. Luminosity $L$ is a quantity to measure accelerator's ability to produce desired events. It is defined as

$$\frac{dR}{dt} = L\sigma, \tag{4}$$

with $dR/dT$ refers to the number of event per second and $\sigma$ as a cross section for such events to happen. It is important to note that Eq. 4 defines luminosity per second or *instantaneous luminosity*. The result has unit of $cm^{-2}s^{-1}$, but the common unit used in particle physics is *barn*. A *femtobarn* of instantaneous luminosity equal to $10^{-36}cm^{-2}s^{-1}$. To get the *total* or the *integrated luminosity* $R$, one needs to integrate instantaneous luminosity over a time period of the beam lifetime $t$.

$$R = \sigma \int_{t}^{t+\Delta t} L dt. \tag{5}$$

Figure 8 shows the increasing trend of energy stored with different bunch crossing configurations. LHC Run-2 used to have a 50 ns bunch spacing in its first months of operation, but switched to 25 ns since August 2015.

1 The bunch spacing indicates the time spacing between proton bunches.

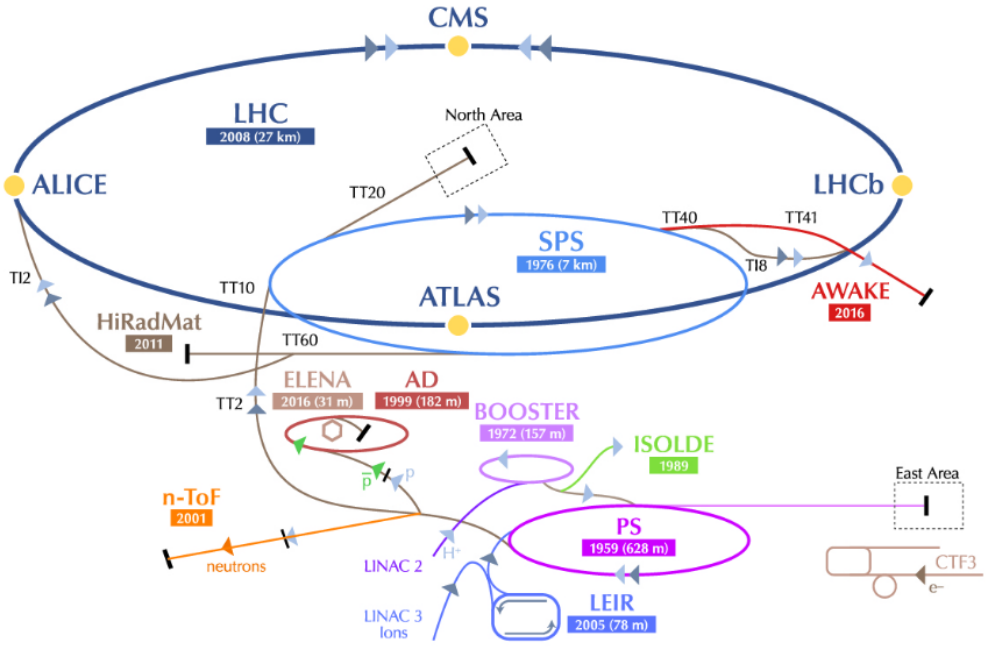


Figure 7: CERN accelerator complex. There are four collision points: ALICE, CMS, LHCb, and ATLAS[16].

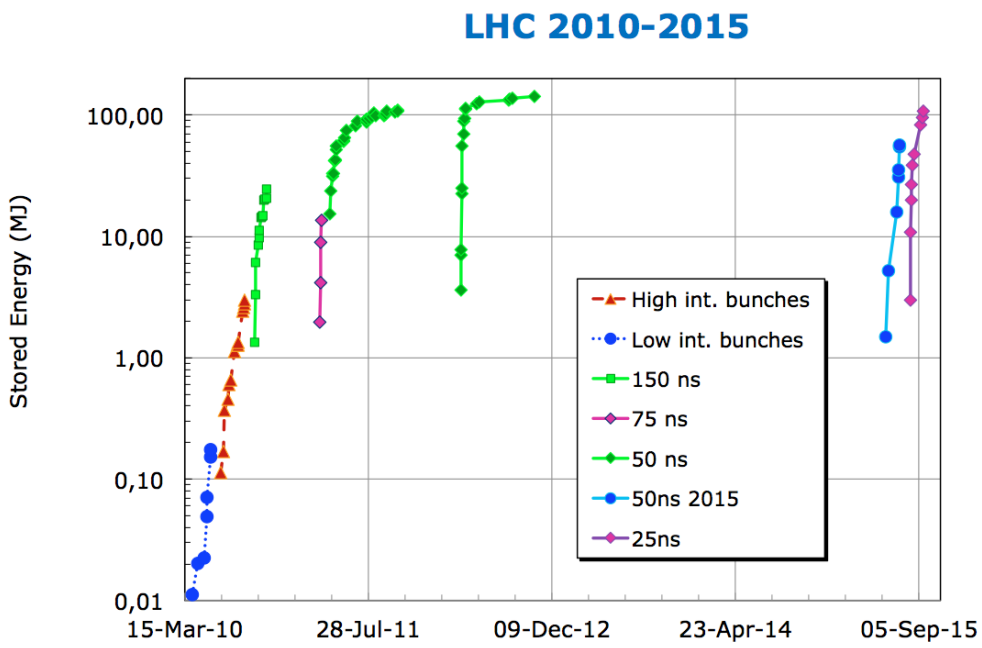


Figure 8: Energy and bunch crossing evolution of LHC from 2010-2015[17].

| RUN | $E_{cm}$ | BUNCH SPACING | INSTANTANEOUS LUMINOSITY |
|---|---|---|---|
| 1 (2012) | 7-8 TeV | 50 ns | $8 \times 10^{33} cm^{-2} s^{-1}$ |
| 2 (2015) | 13 TeV | 25 ns | $1.7 \times 10^{34} cm^{-2} s^{-1}$ |

Table 2: Run-1 and Run-2 specification in machine parameter

As much as 4.2 $fb^{-1}$ of data were delivered by the LHC. Out of those amount of data, only 3.2 $fb^{-1}$ were available for physics analysis with all relevant detectors functioning correctly, as shown in Figure 9. Data taking period in 2015 has ended in November due to the annual heavy ion collisions scheduled to the end of the year.

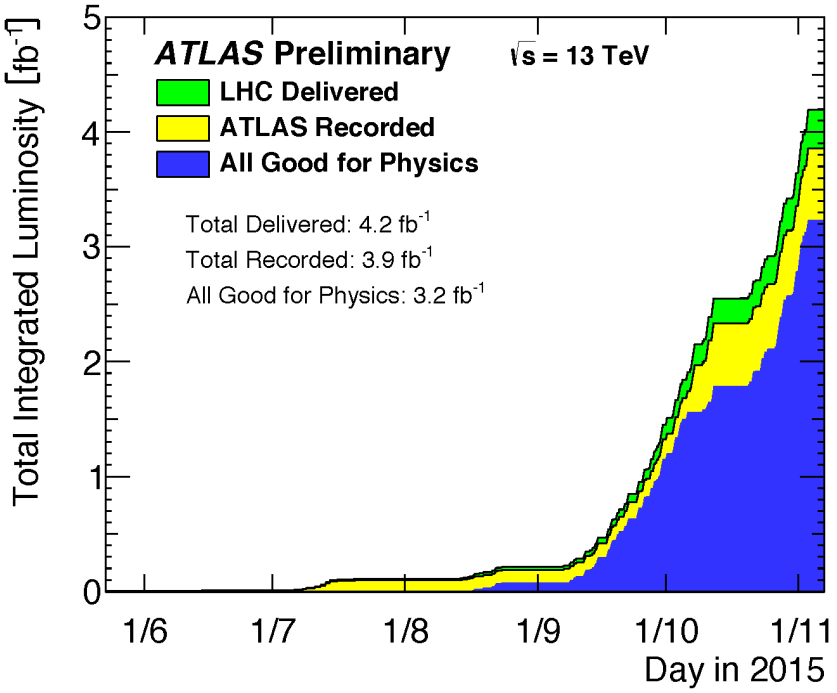


Figure 9: Integrated luminosity plotted against the beam time delivered to ATLAS (green), recorded by ATLAS (yellow), and good quality data (blue) during pp collisions at 13 TeV centre-of-mass energy in 2015[18].

The physics potential in Run-2 is exciting, but it depends on several requirements, such as more efficient computation resources, faster reconstruction phase, and better trigger mechanism. One needs a capable yet versatile detector to maximize the benefit of the new physics potential at 13 TeV, and ATLAS was built with these challenges in mind.

## 3.2 ATLAS DETECTOR

ATLAS is one of the detectors located in the LHC ring. It was designed as a multi-purpose experiment with new physics discoveries as its goal. It can take data both during proton-proton and heavy ions collisions. The ATLAS experiment consists of an inner detector, calorimeters, and muon spectrometer stacked in an onion-like design as shown in Figure 10.

The inner detector gives tracking information, while the calorimeters provide energy measurements. A muon spectrometer sits in the most outside layer of the detector to detect muons. Since this thesis is only focused on the jet physics, only the calorimeters will be explained in detail.

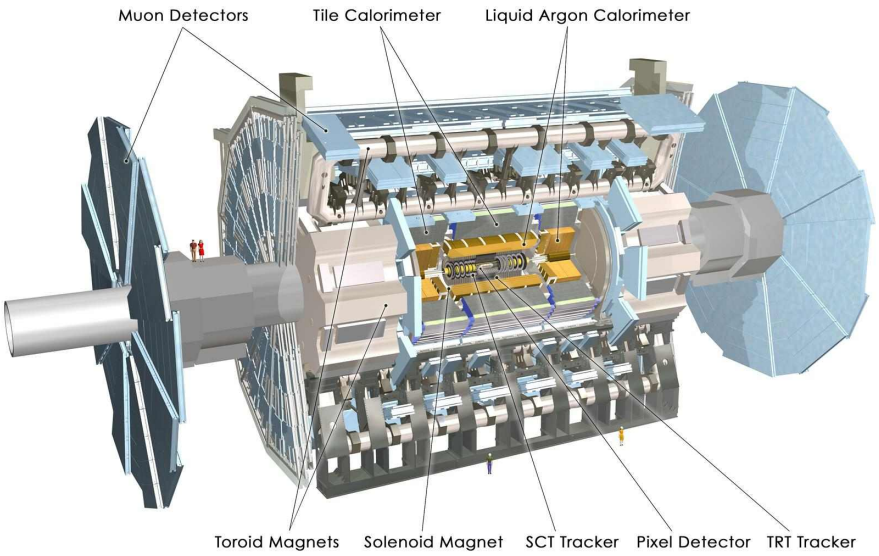


Figure 10: An overview of ATLAS detector with its sub-detectors[19].

### 3.2.1 *Coordinate system*

In the ATLAS coordinate system, the beam acts as the z-axis and the x-y plane is referred as the transverse plane. The x-axis points across the LHC ring and y-axis points across the surface of the Earth. The transverse plane is often described in a coordinate with pseudorapidity $\eta$ and emission angle $\phi$. The $\phi$ angle is measured around the z-axis, while pseudorapidity is a quantity used to simplify the polar angle $\theta$ measurement.

To understand the concept of the pseudorapidity, one can start from the definition of the rapidity itself. The rapidity $y$ is defined as

$$y = \frac{1}{2}\ln\left(\frac{E + p_z c}{E - p_z c}\right), \tag{6}$$

where $E$ is the beam energy and $p_z$ is the particle momentum in the z-direction. Particle with high transverse momentum will have a small $p_z$ value which means $y$ will be close to zero, and vice versa. Rapidity differences are invariant under Lorentz transformations.

Pseudorapidity $\eta$, on the other hand, is defined as

$$\eta = -\ln\left(\tan\frac{\theta}{2}\right). \tag{7}$$

The equation above is easily derived from Eq. 6 by using the fact that particle masses are negligible in relativistic limit. Hence, $y \simeq \eta$ for highly relativistic particles.

One needs to define a distance in $\eta$-$\phi$ plane as $\Delta R = \sqrt{(\Delta\eta)^2 + (\Delta\phi)^2}$. This variable later on will be used to define the radius parameter of the jet algorithm.

### 3.2.2 *ATLAS calorimeter*

The main purpose of a calorimeter is measuring the energy of the incident particles. As the recoil particles from the main collisions strike the calorimeters, their energy is

released and recorded. A calorimeter is designed to absorb energy from most particles, except the muons and neutrinos.

The ATLAS calorimeter contains a *sampling* calorimeter, in which the material for energy measurements is different from the material for enhancing the particle shower. Typically, the two materials are assembled in alternating layers. One advantage of this method is that it can stop the particle shower in a relatively short distance while also providing sufficiently precise energy measurements.

There are two types of calorimeters in ATLAS: electromagnetic (EM) and hadronic calorimeters. The EM calorimeters measure the energy of electrons, positrons, and

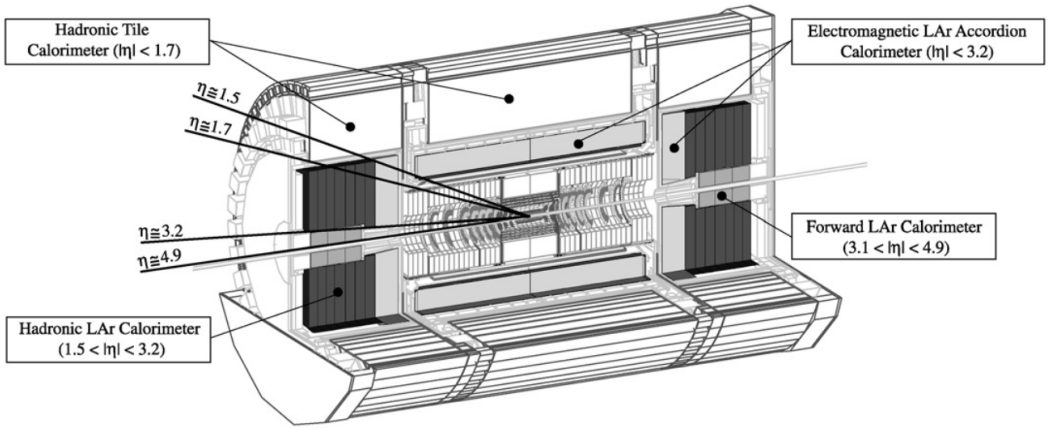


Figure 11: The ATLAS calorimeter. It consists of the electromagnetic and hadronic calorimeter. Some values of η are also shown[20].

photons, while the hadronic calorimeters provide energy measurements for strongly interacting particles. Figure 11 shows the schematic of the ATLAS calorimeters. The EM calorimeters are closer to the inner detector with Liquid Argon as the *active material*, while the hadronic calorimeters use plastic scintillators.

Even though calorimeters are able to stop almost all energetic particles, only a fraction of the particle's real energy will be deposited. A calibration is then needed to convert the deposited energy in the active material into its corresponding real energy.

#### 3.2.2.1 *Electromagnetic calorimeter*

In the electromagnetic calorimeters, electrons and photons interact with the material mostly through *bremsstrahlung* and pair productions. The calorimeter in ATLAS employs alternate layers of lead absorber plates and Liquid Argon (LAr) as an active material which provides the ionizations. The layers are arranged in an accordion-like shape as shown in Figure 12. The calorimeter is divided into a Barrel part that covers $|\eta| < 1.475$ and two End-Caps in $1.375 < |\eta| < 3.2$ This shape was chosen to maximize the $\phi$ coverage without any azimuthal cracks. The thickness for each part is characterized by the *radiation length* $X_0$, an electron's mean distance covered before losing $1/e$ of its energy because of bremsstrahlung.

The structure of the EM calorimeter is divided into three parts: high granularity, bulk, and discriminating calorimeters. The high granularity calorimeter sits closest to the tracking detector. Its main purpose is position measurements and early particle identifications. The next layer is the thickest one as it is where the main shower hap-

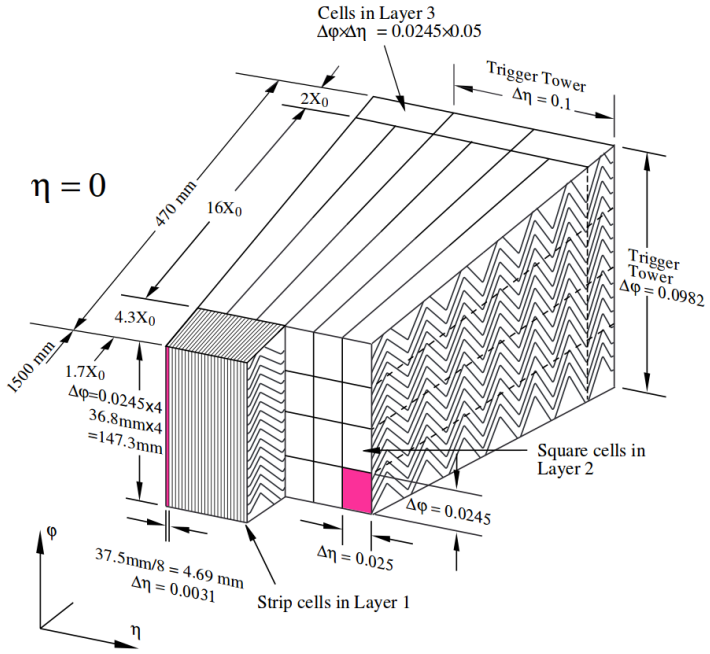


Figure 12: The geometry of electromagnetic barrel module, showing different layers in both lateral and longitudinal directions[19].

pens. Then, the third layer will discriminate further hadronic showers from the EM showers.

#### 3.2.2.2 *Hadronic calorimeter*

Hadronic calorimeter measures particle's energy not only through nuclear interactions, but also through EM interactions. The ATLAS hadronic calorimeters is divided into three parts: Tile Calorimeter (TileCal), Hadronic End-cap Calorimeter (HEC), and Forward Calorimeter (FCal). The TileCal is split into a Barrel and two Extended Barrel regions with coverage of $|\eta| < 1.0$ and $0.8 < |\eta| < 1.7$, respectively. It mainly uses plastic scintillator as the active material. Even though plastic is less resistant to radiation, it provides a precision up to $\Delta\eta \times \Delta\phi = 0.1 \times 0.1$. This is not a problem because the TileCal receives lower radiation due to the screening by the EM calorimeter. Photomultiplier tubes amplify the signal from the TileCal and provide the readout via wavelength shifting fibres.

Both HEC and FCal are LAr sampling calorimeter, each providing different region of measurements. The HEC provides coverage for $1.5 < |\eta| < 3.2$, while the more forward region in $3.1 < |\eta| < 4.9$ covered by the FCal.

#### 3.2.2.3 *Topoclustering*

The ATLAS calorimeter overall can be seen as hundreds of thousands of cells where energy will be deposited. These cells can be assembled into clusters that follow the shower development, building tower-like objects based on the energy deposited. These are called topological cluster, or topoclusters.

ATLAS reconstructs jets in a topological manner. It will try to build a tower-like object based on the structure of the calorimeter cells.

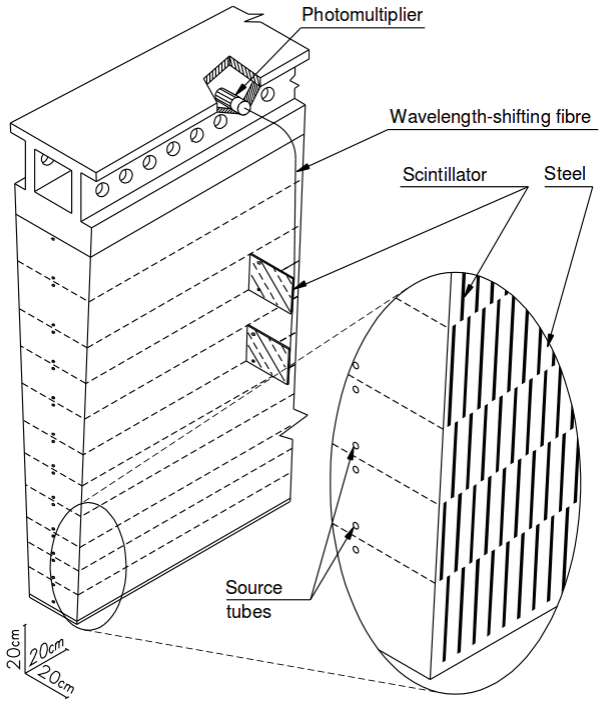


Figure 13: The geometry of the tile calorimeter, showing the alternate layers of the steel and scintillator[19].

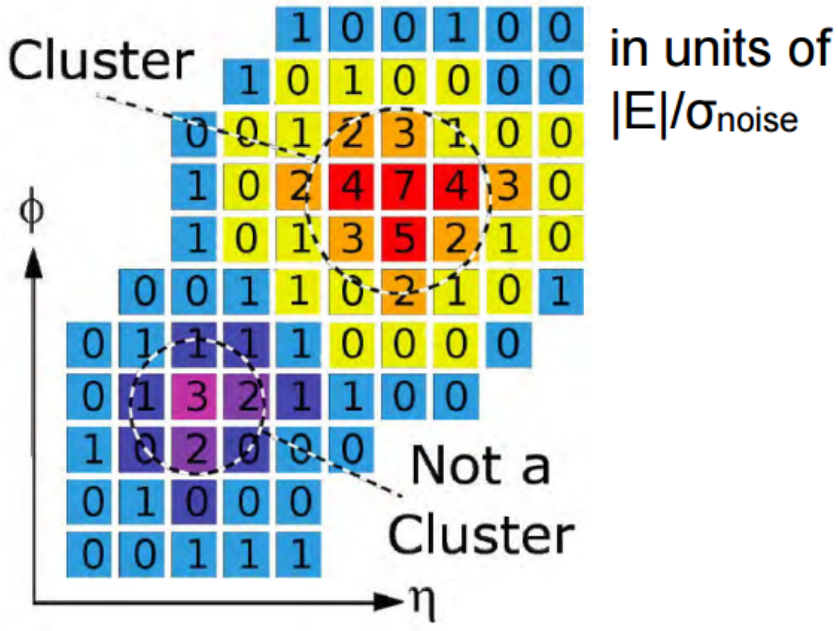


Figure 14: Topocluster algorithm in calorimeter cells. DIfferent colors denote different signal to noise ratio[21].

Figure 14 shows the topoclusters reconstruction process. Every cell hit by particle shower will have an energy measured that can be compared to the intrinsic noise of the cell. A signal to noise ratio is sufficient to trigger the building of topoclusters. At first, the calorimeter will pick up the highest signal to noise cell with value > 4 (marked with red color). Then the calorimeter will scan the nearest cells to choose cells which have energy to noise ratio between 2 and 4 (marked with orange color). Lastly, it will pick any cells around those (marked by yellow color).

## 3.3 JET RECONSTRUCTION

Jet as an object in particle physics is, in general, loosely defined. Its definition as "collimated spray of the high-energy objects" will have different shapes and characteristics, depending on how one reconstruct it. The terms "reconstruction" is referring to a process of building collision data into an object that one could interpret, which in this case is a jet.

One could also view a jet reconstruction as a work of grouping nearby events in $\eta$-$\phi$ space altogether. Visual inspection is, of course, less reliable than algorithm-aided one and almost impossible to perform, given the rate of the collisions. Hence, reconstruction algorithm is needed to build a jet. Formally, this algorithm is defined as

$$d_{ij} = \min(p_{Ti}^{2p}, p_{Tj}^{2p})\frac{\delta R_{ij}^2}{R^2}, \qquad d_{iB} = p_{Ti}^{2p} \tag{8}$$

where $d_{ij}$ is the distance between a pair of objects $i$ and $j$, while $d_{iB}$ is a distance between an object $i$ and the beam $B$. $R$ is the distance parameter of the algorithm with $\Delta R = \sqrt{(\Delta\eta)^2 + (\Delta\phi)^2}$. The $p$ parameter is an arbitrarily chosen parameter to define the jet algorithm. A value of 1 corresponds to $k_t$[22], 0 to Cambridge/Aachen [23], and -1 to anti-$k_t$[24] algorithm. If $d_{ij}$ is the minimum value, the algorithm will keep looking for nearly objects until $d_{iB} > d_{ij}$. ATLAS mainly uses anti-$k_t$because it is collinear and infrared safe. Anti-$k_t$ also performs remarkably well in the detector[24].

There are two kinds of jet reconstructions, online and offline. Both are using topocluster as an input, but the informations that stored in each one of it are completely different. Online jet is reconstructed in the High Level Trigger (HLT) 3.4 by exclusively using detector readout, while offline jet will be reconstructed with full calibration, suppression of noise, and data quality flag applied. The HLT then applies software-based selection on these jets. If it passes the trigger selection, it will be written in physics main stream. On the contrary, Data Scouting (DS) stream will retain all events, either passed the selection or not. Figure 15 illustrates this process.

The physics main stream will have events which are fully reconstructed, while data scouting stream will save only partially reconstructed events. Additional space from DS stream is relatively small compared to the physics main. Therefore, the storage would not be a limitation.

## 3.4 RUN-2 ATLAS TDAQ SYSTEM

One of the areas that has undergone a major upgrade in Run-2 is the Trigger and Data Acquisition (TDAQ) system. This important upgrade is done not only because of a harsher collision condition but also the need for more efficient data taking mechanism.

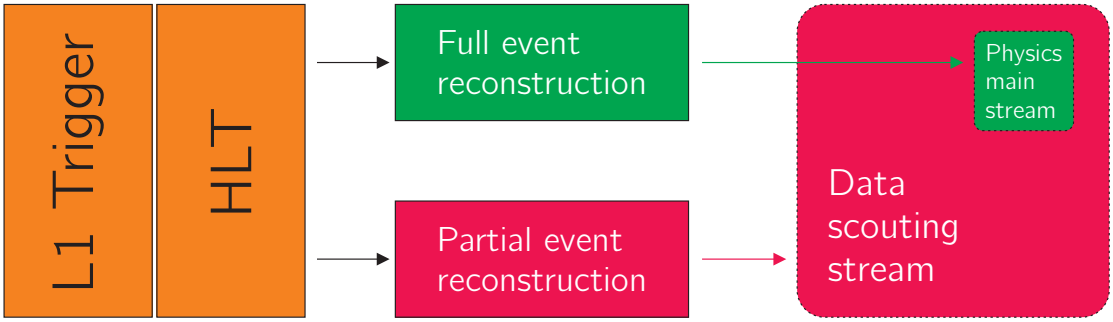


Figure 15: Jet reconstruction procedure for the physics main and data scouting stream. The physics main stream occupies a small subset of the data scouting stream.

### 3.4.1 *Run-2 trigger system*

As mentioned before, ATLAS' performance to probe a new physics, especially for low-mass dark matter mediator particles resonances, will rely heavily on its ability to capture events from collisions. Due to limitations in hardware readout and storage capacity, ATLAS only records a fraction of total data available, employing a multi-stage trigger system to select interesting events.

The most notable change in the Run-2 trigger system is in a unified High-Level Trigger (HLT), removing any distinction between the Level-2 (L2) trigger and the Event Filter like in Run-1. The function of L2 as a processing unit of *Region of Interest* (RoI) from Level-1 (L1) physical trigger and Event Filter as a full event selection unit are unified in a single HLT trigger mechanism. Unified node is favourable because it will reduce HLT resource requirement and only requires a simple software design.

In the hardware-based L1 trigger, jet finding is done by using trigger towers in calorimeter as shown in Figure 12. A jet object is then built with a sliding window algorithm. If certain jet energy threshold is passed, an RoI is created.

The RoI is then used by the HLT to build topoclusters. Finally, an anti-$k_T$ jet algorithm is employed to build a jet which will further be used in the analysis. This scheme is illustrated in Figure 16. A complete sequence of the trigger from L1 to HLT

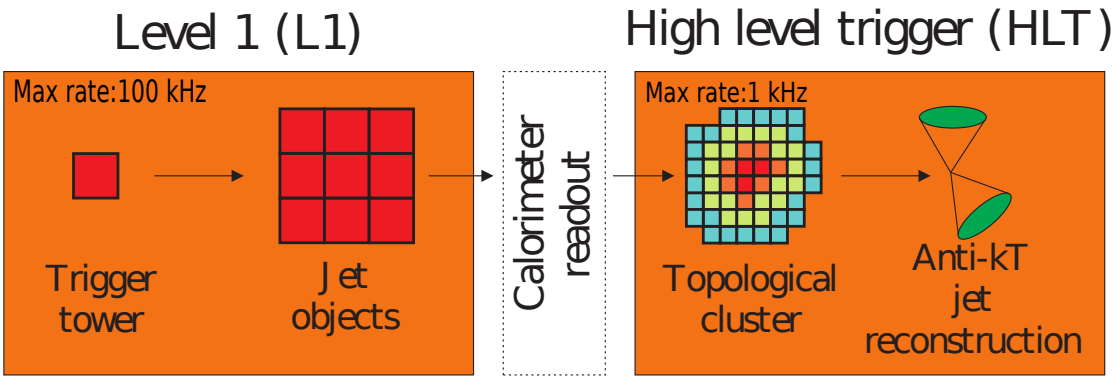


Figure 16: Event building process throughout the ATLAS trigger system in Run-2. L1 is a hardware-based while HLT is software-based trigger.

is often described as a *trigger chain*.

Another addition that is being made is the new Topological trigger (L1Topo). L1Topo will enrich trigger decision with topological information in a way that it can maintain its $p_T$ and prescale threshold. A prescaling refers to the ability of the trigger to select

an event for every n-event. For example, if there is a trigger prescaled with a value of 100, it will only select event once for every 100 events. Certain interesting physics events have their own topological signatures. For example angular distributions topology are useful for identifying jet isolation and b-tagging[25].

A Fast Tracker (FTK) has also started to be developed to reduce the load in HLT in terms of processing tracking information. It will match the particle track information with the pre-assigned data in an associative memory. Hence, the tracking information could be provided in a shorter time compared to the Run-1. The application of the FTK will benefit jet tracking mechanism in the future run. Up until this thesis was written, FTK has not yet been fully utilized.

### 3.4.2 *Data acquisition system*

Data acquisition system as shown in Figure 17 was designed in a simpler way compared to the Run-1. Maximum output readout is 2.4 GB/s. The output of the trigger, called *data stream*, in Run-2 was tidied up to avoid trigger overlap between multiple analysis teams. It is important to note that each team has their specific trigger requirements for their search. However, there is a tendency that multiple triggers will select the same events altogether. This double counting is exhaustive and occupies a big part of the overall trigger bandwidth. Hence, a centralized data stream with a specific menu was developed to maximize the usage of available bandwidth.

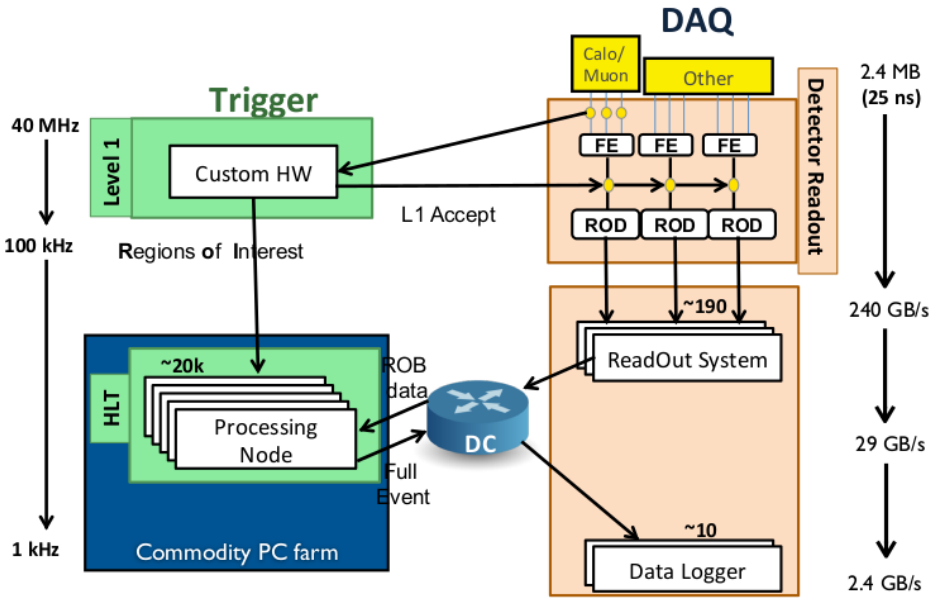


Figure 17: ATLAS Trigger and Data Acquisition (TDAQ) system in Run-2.

#### 3.4.2.1 *Trigger menu*

Table 3 shows some examples of typical physics main stream menu for jets. As a user, one just needs to choose required trigger for their desirable signature. Typical selection shows the current selection that is being made when the lowest unprescaled trigger is fully efficient. Different trigger efficiencies are expected because of various signal characteristics and calibration applied. For example, a Global Sequential Correction

| Trigger | Typical selection | Trigger threshold | | L1 peak rate (kHz) | HLT peak rate (kHz) |
|---|---|---|---|---|---|
| | | L1 (GeV) | HLT (GeV) | | |
| Single jet | Jet (R=0.4) | 100 | 360 | 0.9 | 18 |
| | Jet (R=1.0) | 100 | 360 | 0.9 | 23 |
| Multi-jets | Four jets, each with $p_T > 95$ GeV | 3×40 | 4×85 | 0.3 | 20 |
| | Five jets, each with $p_T > 70$ GeV | 4×20 | 5×60 | 0.4 | 15 |
| | Six jets, each with $p_T > 55$ GeV | 4×15 | 6×45 | 1.0 | 12 |

Table 3: A common trigger menu for singe and multi jets.

(GSC) will improve jet trigger efficiency because it reduces flavour uncertainties from jets.

Jet and dijet use single jet triggers with different radius R of jet algorithm 3.2.1. A 100 GeV cut in the L1 trigger is applied as a preliminary selection for those triggers. The lowest unprescaled trigger $p_T$ in the main stream is set to 360 GeV.

However, in the experiment, jet trigger is not as trivial as stated above. There are different options for each of the jet triggers that are being used for specific purposes such as commissioning, calibration, and data monitoring stream. The commissioning phase refers to the application of the jet trigger in a cosmic-ray and technical runs. On the other hand, the calibration phase uses multi-jet trigger for offline jet calibration purpose. The data monitoring, or *express* stream, uses low rate trigger to select a small fraction of total data to be reconstructed quickly before physics main stream finished. One could spot detector problem and determine the quality of the data by using this stream.

#### 3.4.2.2 *Trigger naming scheme*

A subtle distinction between different triggers is important for the user in order to address its feature quickly. This feat could be achieved by providing a simple naming scheme for the trigger chain.

The trigger chain name always started with the trigger type, followed by the $p_T$ threshold and (but not always) the pseudorapidity range. An absence of $\eta$ from the trigger chain name refers to $\eta$ from 0 to either 2.8 or 3.2, depending on the availability of the menu for forward region [26]. L1 seed also could be added afterwards.

For example, multijet trigger chain 6j45_0eta240_L14J20 is translated as a trigger for 6 jets with minimum transverse momentum of 45 GeV in an $\eta$ range between 0 and 2.4 seeded by L1 trigger of multijet with each jet $p_T$ more than 20 GeV. More options and full naming scheme are available in [26].

#### 3.4.2.3 *Data scouting stream*

The lowest unprescaled jet trigger is limiting ATLAS' ability to probe low-mass hadronic final states. There is a risk that important events could be discarded by a heavy prescaled conditions. Fortunately, the limitation of ATLAS is stricter on the computing

resources than *not* the storage. It gives birth to the idea of data scouting. Data scouting stream is using a looser selection so that the trigger can have more events even though with less information.

Since bandwidth is the main limitation of data readout in the ATLAS, reducing event size will automatically improve event rates. Data scouting only records limited amount of information as a bid to reduce its event size. With a small event size, prescaling is not needed anymore. Hence, there is a jump in sensitivity for events with $p_T$ as low as 180 GeV. Figure 18 shows the comparison between the DS and physics main stream. A significant difference is dominant in the region below 360 GeV as the lowest unprescaled trigger. The DS stream records ten times more events compared to usual single jet trigger.

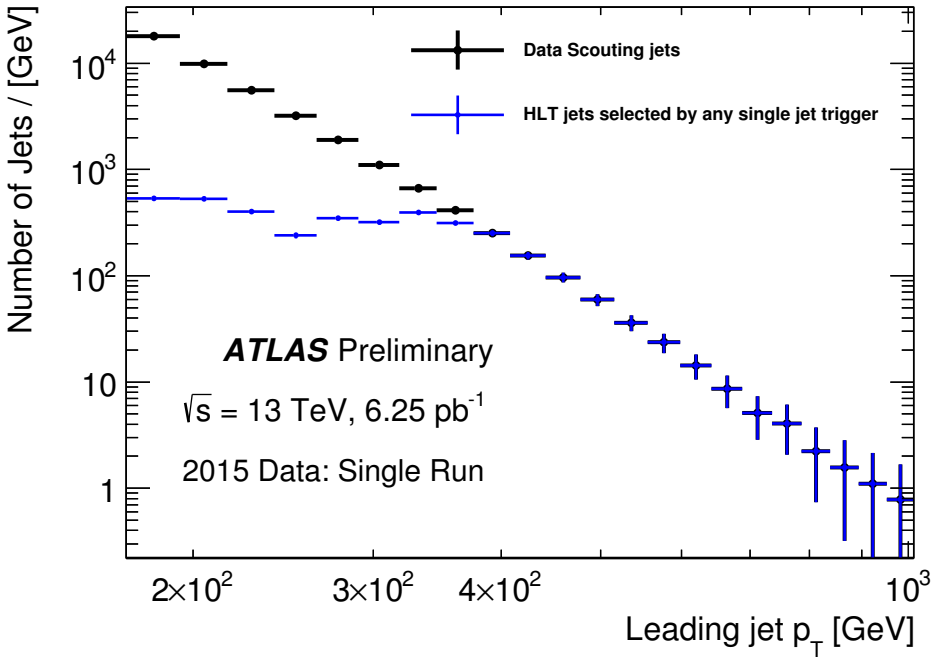


Figure 18: A comparison of the transverse momentum distribution between the leading HLT jets from data scouting stream (Data Scouting jets) and physics main. All the jets from physics main are recorded with single jet HLT trigger in a single run. Data scouting jets have a higher statistics in the region below 400 GeV because it does not need to apply prescale factors, which is normally applied in the main stream.

## 3.5 DATA PROCESSING IN ATLAS

However, not all data produced by the LHC is good enough to perform an analysis. Broken calorimeter cells, unstable beam, or low instantaneous luminosity condition are some of the causes of low data quality. A quality tag, or *lumiblocks*, is given beased on the duration of the collision. LHC then collects all those lumiblocks and makes a `GoodRunList` (GRL). GRL will be used in most of the analysis algorithm to discard data with poor quality.

Different requirements are set throughout the data processing sequence, and it is different between one and each other. In the very first step of data taking, one wants to record data as much as possible. However, once it was processed and reconstructed,

efficient usage of the resources is the main goal. Not all information in the physics main stream is relevant for analysis teams. Each of them has their own interests and desirable signatures that often only occupied a small fraction of the data stream. A process on reducing size by discarding unnecessary information, tidying data structure, and optimizing performance is called *derivation*. *Derived Analysis Object Data*, or *DAOD*, are usually stored in a distributed computer grid across the world. User in the collaboration can further run their analysis without the need to prepare a terabyte-scale local storage. The resulting files usually have a much smaller size which fit typical personal computer.

However, one cannot just applies typical offline reconstruction technique on the data scouting stream due to limited information available. One needs to define a dedicated reconstruction and calibration strategy for it. This will be addressed in the Chapter 4.

# 4

# TRIGGER LEVEL ANALYSIS

The Trigger Level Analysis (TLA) is an analysis which performed by using High-Level Trigger (HLT) objects collected from the Data Scouting (DS) stream. This chapter will focus on the use of a TLA as a new strategy to overcome limitation and challenge of probing new physics in the low-mass region. Section 4.1 will give an introduction to Trigger Level Analysis. The calibration sequence will be described in the Section 4.2 and the validation method will be presented in Section 4.3.

## 4.1 TRIGGERING STRATEGY FOR TLA

The TLA is designed to utilize the reduced event format recorded in the Data Scouting (DS) stream to perform an analysis. In this stream, more events are recorded because the event size is smaller. This is achieved by reading out a small fraction of information from the calorimeters only, and building jets from these inputs. To understand this concept, let us define bandwidth as

$$bandwidth = event\ rate \times event\ size. \tag{9}$$

It means that the TLA events, which have a size of 30 Kb/events, can have a significant improvement on rate compared to fully reconstructed events with a size of 1 MB. Figure 19 shows the rate of the DS stream which is seeded by L1_J75. DS stream in red has a difference of a factor of 10 compared to the rates of all single triggers.

In 2015 run, DS stream was filled by trigger chain jo_perf_ds1_J75. One could notice that this chain was using pretty unusual naming scheme by an addition of "perf", an abbreviation of "performance". The reason for that is because DS trigger was still considered as a test run in 2015. Hence, it was classified as a commissioning trigger because its partially-reconstructed nature and the fact that this stream is different from the usual physics main stream. Further, in the 2016 run, the DS stream could be having a higher rate by employing 20 GeV cut in trigger jet to reduce the event size to 10 Kb/event[27].

## 4.2 JET ENERGY CALIBRATION

A Jet as a theoretical object is different from a jet that one measures in the experiment. A jet as a conceptual object is the result of the hard-scattering process. This can be reconstructed from Monte Carlo simulation, and in the following passage it will be called *truth jet*.

Since it is simulated as a product of p-p collisions with known energy, a truth-jet has the correct *Jet Energy Scale (JES)*. Therefore, one can use truth jets as a reference in Monte Carlo to bring the energy scale of the experimental jet as close as possible to their matched truth-jet counterpart.

The ratio between the reconstructed jet and truth-jet energy is defined as

$$R = \frac{E^{reco}}{E^{truth}}. \tag{10}$$

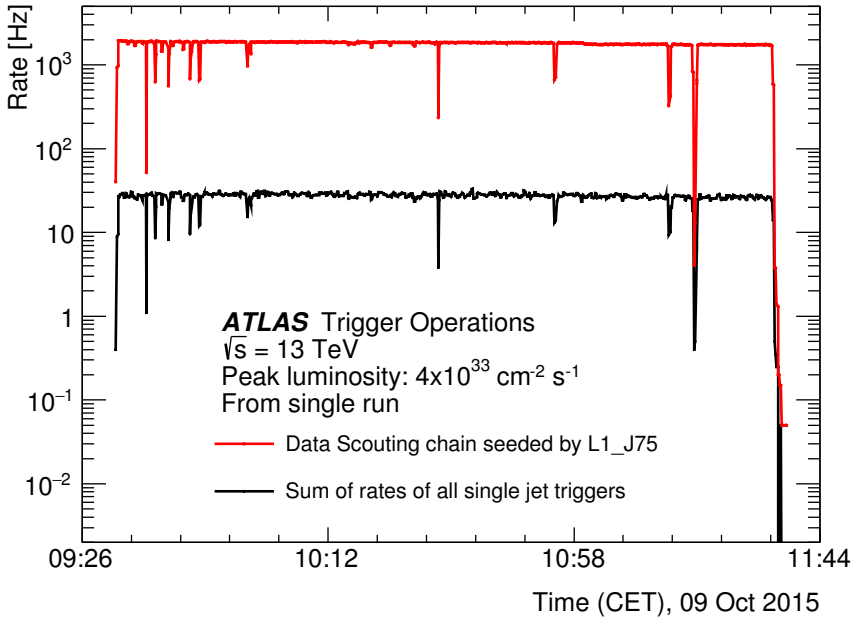


Figure 19: Trigger rate for the data scouting chain seeded by the Level-1 trigger J75 compared to the sum of the rates of all central single jet triggers, plotted against a time range of a single run. DS chain has more statistics due to smaller event size recorded.

It will be a parameter to measure jet energy response. Normally, it will have a value less than one with a resolution spread because of detector effects, such as dead material before the calorimeters. Furthermore, pile-up adds energy to jets due to extra collisions 4.2.1.

To overcome these issues, ATLAS developed a sequential calibration scheme which is divided into three parts: pile-up suppression, JES correction, and in-situ calibration. The pile-up suppression process makes sure the jet response does not change, regardless the number of primary collision vertices. Then, the JES correction, which is an MC-based calibration, aiming at restoring the reconstructed jet energy response to the truth jet level. Finally, the in-situ calibration will bring the jet energy response of jets from the experiment into an agreement with the MC jets, overcoming the possible problems in the modelling of the Monte Carlo simulation. Figure 20 illustrates this process.

As opposed to the fully reconstructed jets, HLT jets are built only from calorimeter inputs. Applying standard offline calibration is not possible due to the lack of tracking information. Moreover, the JES calibration applied to the HLT jets when they are recorded is not optimal as it is derived from a Run-1 MC sample. Figure 20 highlights the difference in the calibration process between online and offline jets. Different color specifies the required information that is needed to perform those calibrations. For 2015 run, only calorimeter-based calibrations are performed. The Global Sequential Correction (GSC) to reduce differences in response between quark and gluon jets can also be performed partially from calorimeter input, but it is not applied in this analysis. What can be done to improve the performance of HLT jets is to use a well reconstructed object, the offline jets, as a baseline. Being as close as possible to the offline jets is the main goal of the dedicated calibration sequence studied in this thesis.

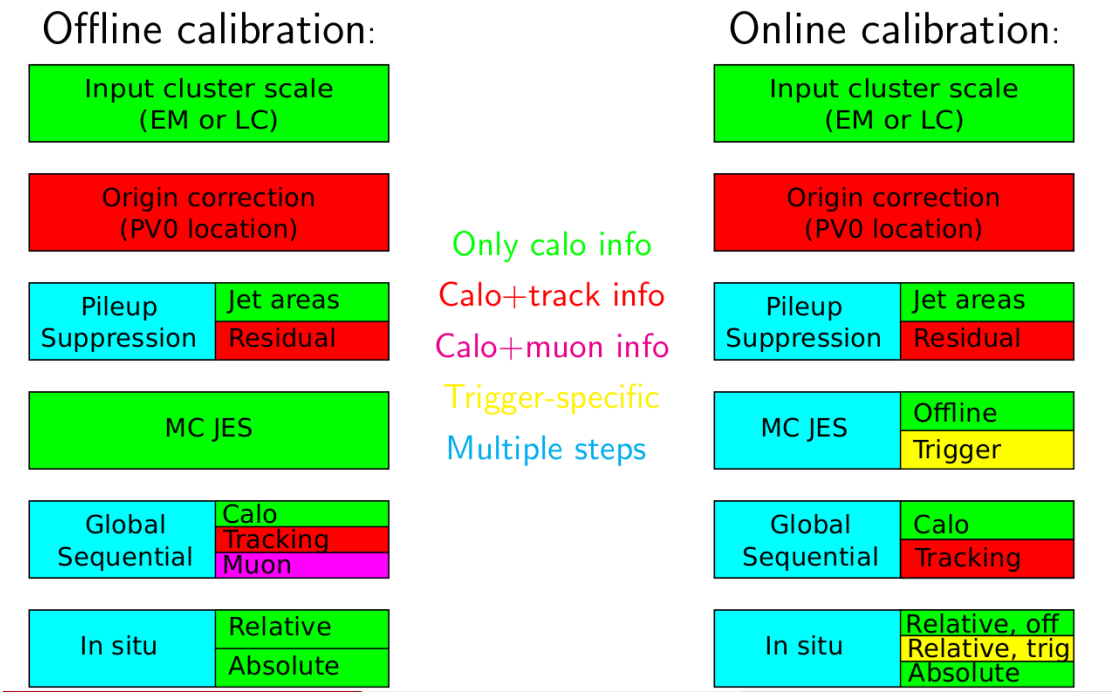


Figure 20: A comparison between offline and HLT (online) jets calibrations. Different colors marked different information needed for it to be applied.[28]

### 4.2.1 *Pile-up correction*

Pile-up happens when there are additional collision within the bunch crossings. It is poses as a challenge in collider physics especially at the high instantaneous luminosities collision environment at the LHC. Its impact can be reduced by using topological clustering and a so-called *jet area* subtraction method. By using a signal to noise ratio in the topoclustering, accounting for both calorimeter and pile-up noise, one can reduce pile-up significantly at the level of jet inputs. Then an event-by-event subtraction based on the jet area could be applied. The jet area method uses $\rho$, the median of $p_T$ density in the whole event, to provide an estimation of the pile-up activity in each event. The jet area $A$ itself is used to subtract this extra energy from the jet. The correction is defined as

$$p_T^{corr} = p_T^{jet} - \rho \times A. \tag{11}$$

An additional *residual correction* is applied only to the offline jets because HLT jets does not have tracking information. This residual correction will have a sizable effect in low $p_T$ region. Fortunately, the unavailability of the residual correction does not introduce any problem because TLA selects leading jet with $p_T > 185$ GeV. The second jet will have a similar average $p_T$ to balance the leading jet - this will reduce the impact of low-$p_T$ jets in the analysis.

Figure 21 shows the robustness of trigger level analysis to pile-up. The value of average dijet invariant mass is relatively flat, even though the number of the primary vertex (NPV) keeps increasing.

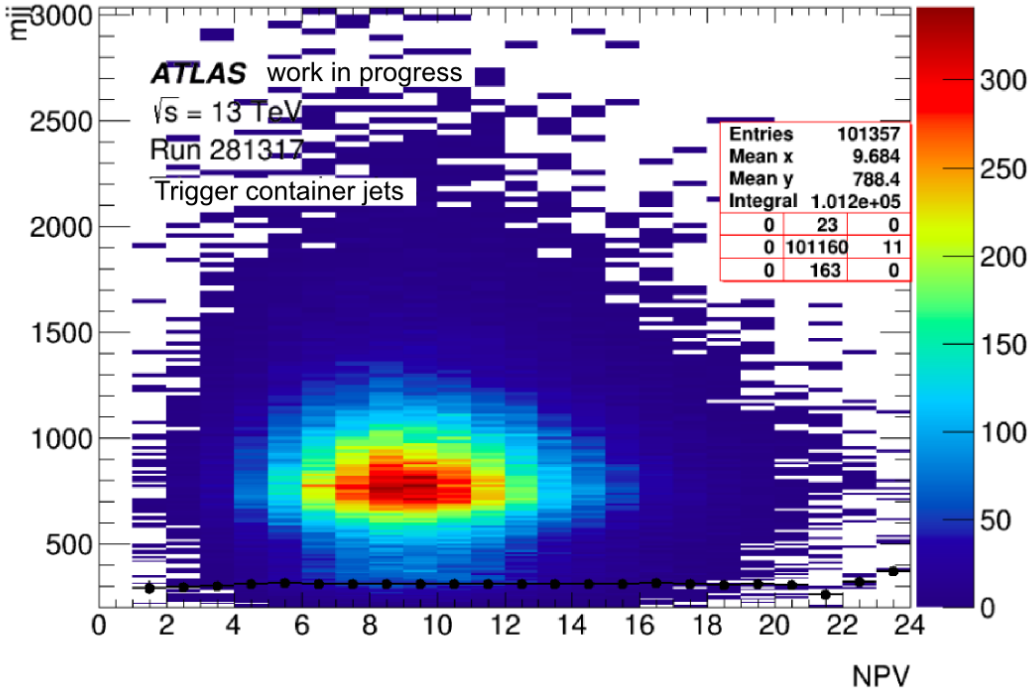


Figure 21: Dijet invariant mass distribution as a function of the number of primary vertex(NPV). The black points denote the average value of the dijet invariant mass.

### 4.2.2 *Jet energy scale correction*

The JES correction is calculated as a factor that relates reconstructed and truth jet energy. This correction was derived by applying pile-up subtraction from Monte Carlo samples and then inverting the jet response through numerical inversion technique[27]. The original JES correction applied to online jets was derived from the outdated MC12 sample. Therefore, a new calibration derived from MC15 samples is necessary in order to reduce the JES uncertainties.

Figure 22 shows the $p_T$ ratio between online and truth jets, as a closure test after applying this calibration. Less than 1% difference was observed across all $p_T$ regions.

Figure 23 shows the transverse momenta comparison between online and offline jets. The calibration performs well and the response of HLT jets only differs 2% from the offline one in the central region of the detector.

However, a closure test to match the $p_T$ of HLT and offline jets in figure 24 shows high detector dependencies. Big differences are observed and marked with orange and red colors. Strong spikes in the transition area between central and forward region were expected because of different quality of signal generation between those two regions.

### 4.2.3 *Residual in-situ correction*

A residual in-situ correction aiming at bringing agreement between data and MC. It is defined as

$$\mathrm{JES}^{\mathrm{insitu}} = \frac{(p_T^{\mathrm{jet}}/p_T^{\mathrm{ref}})_{\mathrm{MC}}}{(p_T^{\mathrm{jet}}/p_T^{\mathrm{ref}})\mathrm{data}} \tag{12}$$

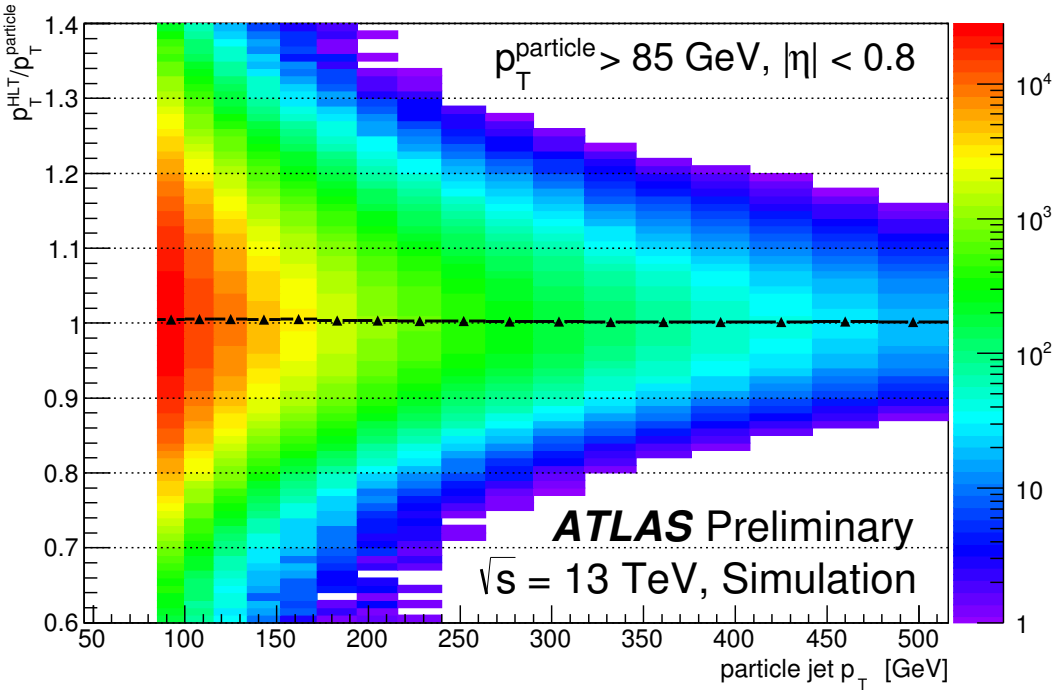


Figure 22: Transverse momentum plot of the HLT and truth jets after correcting HLT jets for pile-up and jet energy scale correction factors.

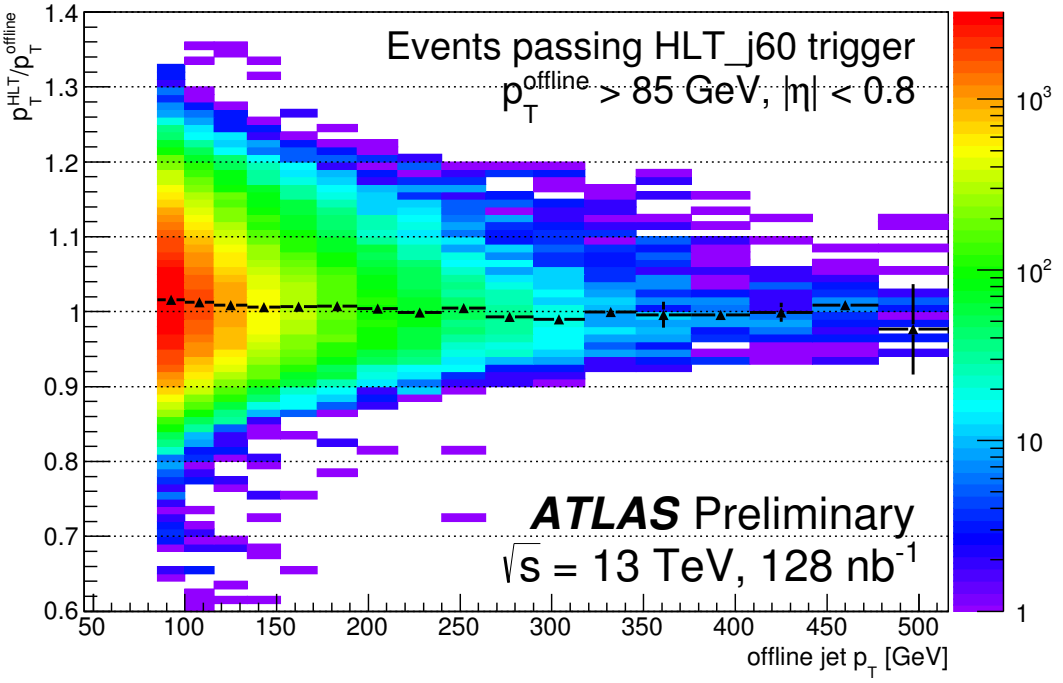


Figure 23: Transverse momentum plot of the HLT and offline jets after correcting HLT jets for pile-up and jet energy scale correction factors.

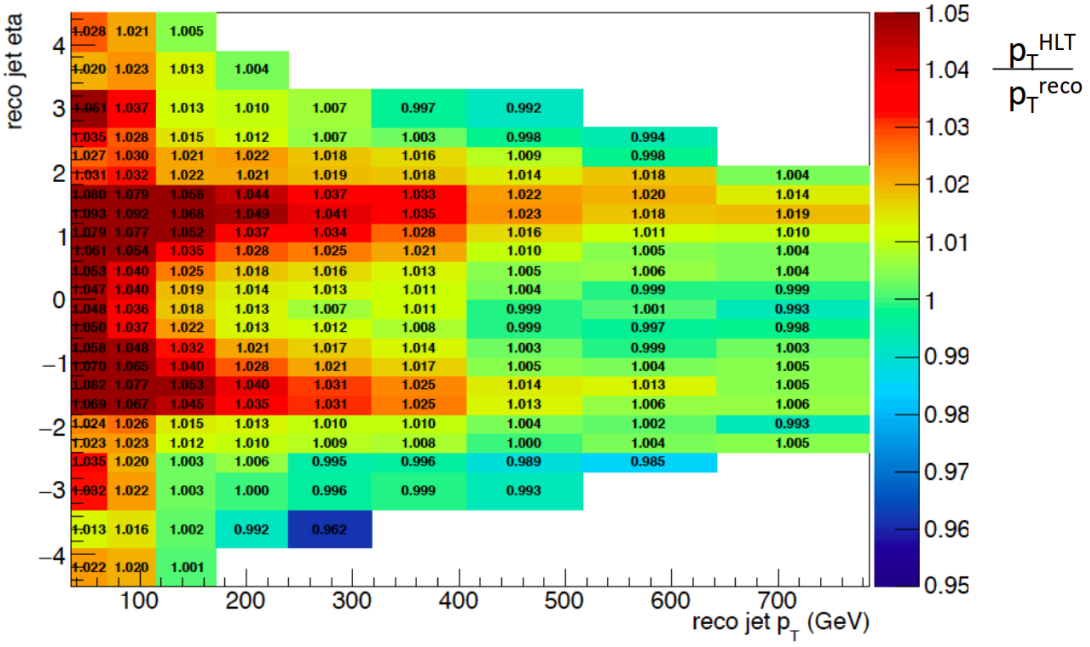


Figure 24: A closure test between HLT and reco jets.

where the reference must be a well-calibrated object, either photon, Z boson, or another jet. In general, there are three steps of applying in-situ correction. First, one balances the detector response between central and forward region. Next, photons and Z bosons recoiling against the jets are used to balance central jet $p_T$. Lastly, the final step of calibrating high-$p_T$ object could be performed by using multijet events. However, only the first phase is applied in TLA. This is because $\gamma$ and Z boson are not available in the data format EXOT2 that being used. This is happens mainly because EXOT2 were made specifically for jet-related search and not lepton-based search.

### 4.2.4 *Eta inter-calibration*

As mentioned in Section 4.2.2, there are detector-dependent differences in the jet energy scale after applying the MC-based JES calibration. On Figure 24 one can clearly notice that the forward region tends to have a worse energy response compared to the central region. This problem needs to be addressed with relative $\eta$-dependent calibration by exploiting the dijet balance technique. Both central reference and matrix method will be described in this Chapter[29][30].

#### 4.2.4.1 *Central reference method*

In the central reference method, $p_T$ of the jet in the central region (($|\eta|$<0.8)) acts as a *reference jet* $p_T$ ($p_T^{ref}$). Central jets are chosen as the reference because they have uniform jet responses. The reference jet balances a *probe jet* in the forward region. Due to the transverse momentum conservation, both reference and probe jets should have an equal $p_T$. The $p_T$ balance is described by the asymmetry $A$:

$$A = \frac{p_T^{probe} - p_T^{ref}}{p_T^{avg}}, \tag{13}$$

where $p_T^{avg} = (p_T^{probe} + p_T^{ref})/2$ denotes the average $p_T$ value of two jets. In case both jets are in the central region, one could, in turn, arbitrarily chose a probe or reference. This will make sure that the asymmetry in the central region stays zero, which means that there will be no correction applied.

Once it is calculated, the asymmetry is then used to derive an $\eta$ inter-calibration constant $c$ for the probe jet. The response ratio between the probe and the reference jets then can be calculated as

$$\frac{p_{Tik}^{probe}}{p_{Tik}^{ref}} = \frac{2+\overline{A_{ik}}}{2-\overline{A_{ik}}} = 1/c_{ik}, \tag{14}$$

where the average asymmetry distribution $\overline{A_{ik}}$ is computed for each $\eta$-bin $i$ and $p_T^{avg}$-bin $k$.

#### 4.2.4.2 *Matrix method*

The central reference method performs well for the case when there is at least one jet falls in the central region. For this reason, it will suffer from low statistics, especially if both jets fall in the forward region. Low statistics is not favourable because it introduces higher uncertainties in the correction factors. In order to obtain more statistics, one can replace "reference" and "probe" jets by "left" and "right" jets defined as $\eta^{left} < \eta^{right}$. In this method, multiple reference region could be used to measure the jet response. Therefore, more statistics is available for calibration. Equations 13 and 14 are then need to be slightly modified:

$$A = \frac{p_T^{left} - p_T^{right}}{p_T^{avg}} \tag{15}$$

where the response ratio is defined as

$$\frac{c^{right}}{c^{left}} = \frac{2+\overline{A_{ik}}}{2-\overline{A_{ik}}} = \overline{R}. \tag{16}$$

The $c^{right}$ and $c^{left}$ denote the $\eta$ inter-calibration constant for the right and left jets, respectively.

The response ratio distribution $R_{ijk}$ with mean value $\overline{R_{ijk}}$ is evaluated for every $\eta^{left}$-bin $i$, $\eta^{right}$-bin $j$, and $p_T^{avg}$-bin $k$. A minimization matrix then can be used to calculate $\eta$-intercalibration constant $c_{ik}$ for a number of $\eta$ bin $N$:

$$S(c_{1k}, ..., c_{Nk}) = \sum_{j=1}^{N} \sum_{i=1}^{j-1} \left(\frac{1}{\Delta\overline{R_{ijk}}}(c_{ik}\overline{R_{ijk}} - c_{jk})\right)^2 + X(c_{1k}, ..., c_{Nk}), \tag{17}$$

where $\overline{R_{ijk}}$ denotes the statistical uncertainty of $R_{ijk}$. The function $X(c_{ik})$ itself will prevent the minimization from choosing the trivial solution $c_{ik} = 0$. The resulting calibration constant also needs to be scaled properly in order to have zero correction in central region.

## 4.3 JET ENERGY SCALE VALIDATION

The HLT jet calibration can be validated *in-situ* using the multijet balance technique. Multijet is the only available technique to cross-check the calibration at the moment due to the absence of photons in the data format used for the analysis.

The multijet balance technique selects events with back-to-back balanced jet topologies, with one highest $p_T$ jet (leading jet) in one direction and other lower $p_T$ jets in the opposite directions (non-leading jets). Figure 25 shows the event topology for the multijet event.

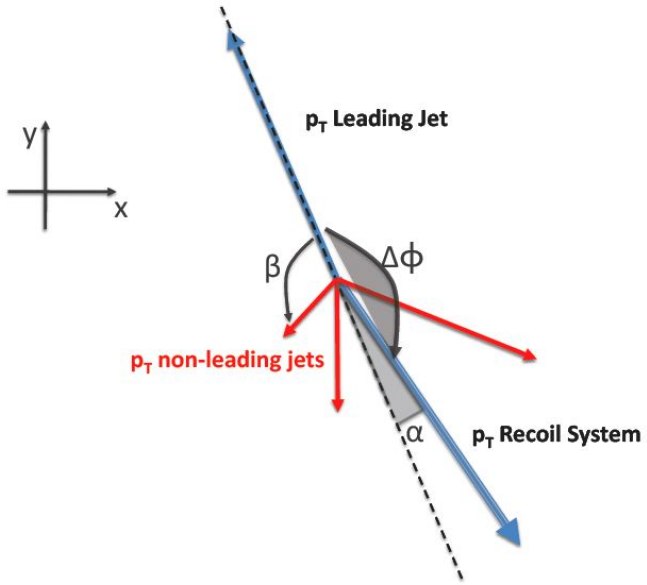


Figure 25: The topology of a multijet event[31].

The $p_T$ of the non-leading jets is then added together to form a $p_T^{recoil}$. The transverse momentum of the recoil jets will balance the leading jet $p_T^{leading}$. Therefore, the multijet balance (MJB) can be defined as

$$MJB = \frac{p_T^{leading}}{p_T^{recoil}}. \tag{18}$$

The ideal MJB will have a value close to unity. However, various effects from trigger turn on, pile-up, and the presence of nearby jets could introduce biases in the result.

# 5

# RESULT AND DISCUSSION

This chapter provides a discussion of the result obtained in this thesis. It starts with the basic event selection in Section 5.1. A detailed result of the calibration with selected $p_T^{avg}$ bins is then presented in Section 5.2. Then, Section 5.3 explains the multijet balance validation method.

## 5.1 EVENT SELECTION

The term "dataset" in ATLAS is not only limited to the real experimental data but also refers to simulated MC. An experimental dataset name always starts with "data" followed by the year of the generation and the center of mass energy such as "data15_13TeV". The same rule applies to simulated data, with an example of "mc15_13TeV". Every dataset is equipped with a set of self-explained information called metadata. It is maintained by the ATLAS metadata tools in [32] and [33].

### 5.1.1 *Real data*

This analysis uses both the main physics stream (where events are fully reconstructed) and Data Scouting stream with different purposes. The main physics stream has both online and offline jets that passed the HLT trigger, while the DS stream only has HLT jets. The HLT jets from DS stream will be matched and compared with offline jets from the physics main.

The TLA uses Derived AODs (DAODs) data format from the main physics stream in the form of EXOT2 with sample production tag p2425 and JETM1 with tag p2425 or p2440. EXOT refers to a derivation that belongs to the exotics group while JETM belongs to the jet-Etmiss group. Further, DS stream with a tag r7370_p2424 is used as a source of online jets for this analysis.

All data marked as Good Run List with tag DetStatus-v73-pro19-08_DQDefects-00-01-02 for 2015 run with total luminosity 3.2 $fb^{-1}$ will be used.

### 5.1.2 *Simulated data*

There are two event generator used in this thesis. The first one was a combination between Powheg[34] and Pythia8[35] with tag p2352. It was tuned with A14 and NNPDF 2.3 LO and CT10ME PDF parameter set[36]. The parameter set is acting as a setting for the simulation that will determine the outcome of the simulation. It is usually chosen to make the simulation as realistic as possible. The second one was Sherpa with tag p2440 and CT10 PDF parameter set [37]. Both generators later on will be compared with the data and one can investigate the agreement between data and MC.

### 5.1.3 *TLA selection*

TLA uses trigger jets that were built with anti-$k_t$ algorithm from topocluster input with radius R=0.4. An event will be selected if it has at least a dijet event with $|\eta|$<2.8 and minimum $p_T$ of 50 GeV. The angular separation y* < 0.6 was chosen, where y* as the average rapidity between 2 jets is employed to make sure that the dijet is a back-to-back event. This value was chosen to maximize signal to background ratio [27].

In order to have fully efficient L1_J75 trigger, a $p_T$ cut was used to remove events with leading jets below 185 GeV. An event will be kept if it has a second jet with $p_T$ > 85 GeV.

The selection of jets for deriving the $\eta$ intercalibration constants is then applied. The dijet events should have $\triangle\phi$>2.5 to suppress soft-radiation. In order to reduce pile up, a JVT (jet-vertex-tagger) value, which measures the fraction of total momentum of tracks in the jet with regards to the primary vertex, should be more than 0.64, while the third leading jet $p_T$ should have below 40% of $p_T^{avg}$ to maintain the event topology.

## 5.2 ETA INTERCALIBRATION RESULT

### 5.2.1 *Eta binning*

Figure 24 demonstrates the binning ($\eta_{det}$, $p_T$) strategy used in this analysis. The binning was designed with a goal to have similar statistics in each $p_T$-bin. Lower $p_T$ tends to have lower statistical precision due to prescaling and worse jet resolution from wider asymmetry distribution. One also needs to be careful with high $p_T$ bins because they have lower number of entries due to the decreasing cross-section.

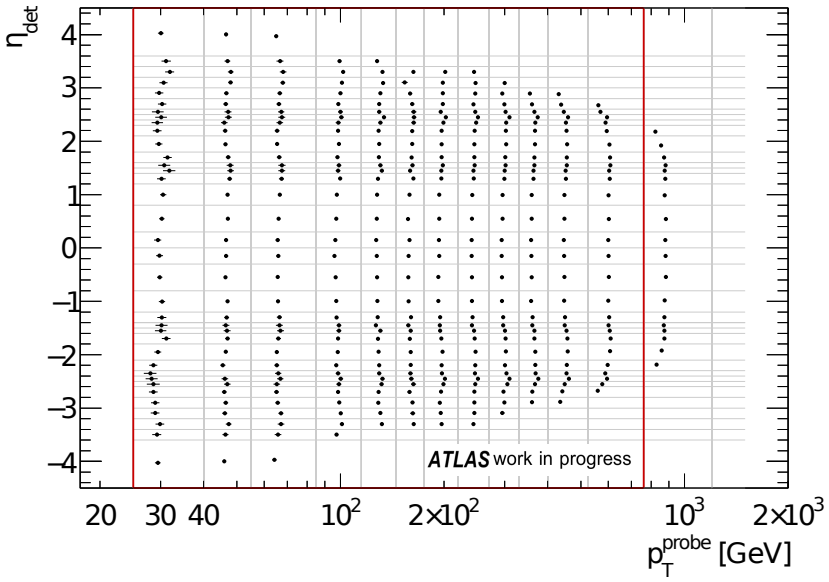


(a)

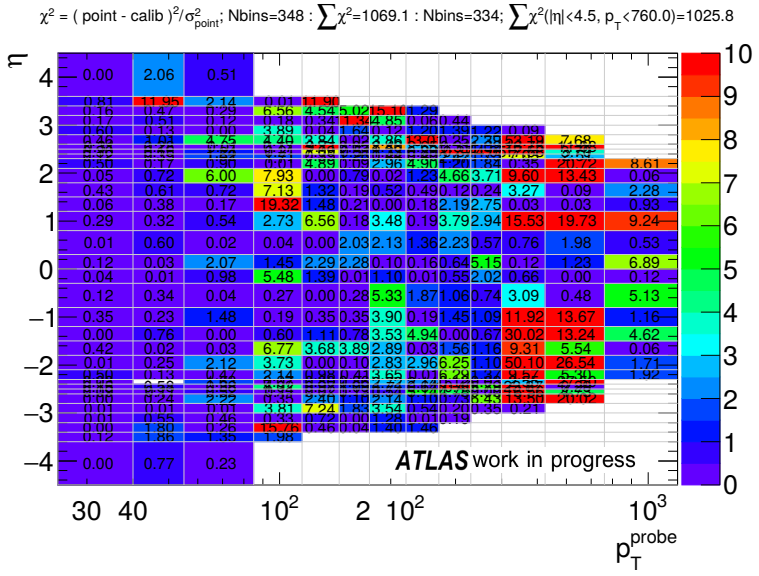


(b)

Figure 24: Binning that is being used in η intercalibration.

A feature that also needs to be addressed is the problematic η region where the spikes are observed earlier in Figure 24. This analysis is using finer binning in η=1.4,2.4. In those regions, bin width of 0.1 was chosen and 0.2 otherwise. A finer binning is useful for more detailed study of the trend in that region. However, it also carries a risk of having low statistics within that bin at the same time. If the number of entries in a bin is too low, there will be no enough points to make an asymmetry histogram and fit it properly. In this analysis, a chi-square fitting also performed as a complement to the more common method of taking the mean and Root-Mean Square (RMS) of the distribution. Both binnings are shown in Figure 26a and 25b for original and chi-square, respectively. A reasonably uniform binning was obtained after attempting multiple binning configurations.

### 5.2.2 *Comparison of η inter-calibration method*

Figure 25 shows the relative response distribution comparison between data and MC samples. Two $p_T^{avg}$ regions are chosen: $85 \leqslant p_T^{avg} < 115$ GeV, and $175 \leqslant p_T^{avg} < 220$ GeV. The first region represents the lowest available $p_T$ in DS stream which is seeded by L1_J75. On the other hand, the second region represents a $p_T$ range where the TLA trigger is fully efficient[27]. In general, matrix method results in Figure 25b and 25d give slightly higher relative responses with lower error bars. This result is expected because matrix method has higher statistics. It is also observed that this observation agrees with other studies[29][30]. Hence, the matrix method is preferred to derive relative response in this analysis.

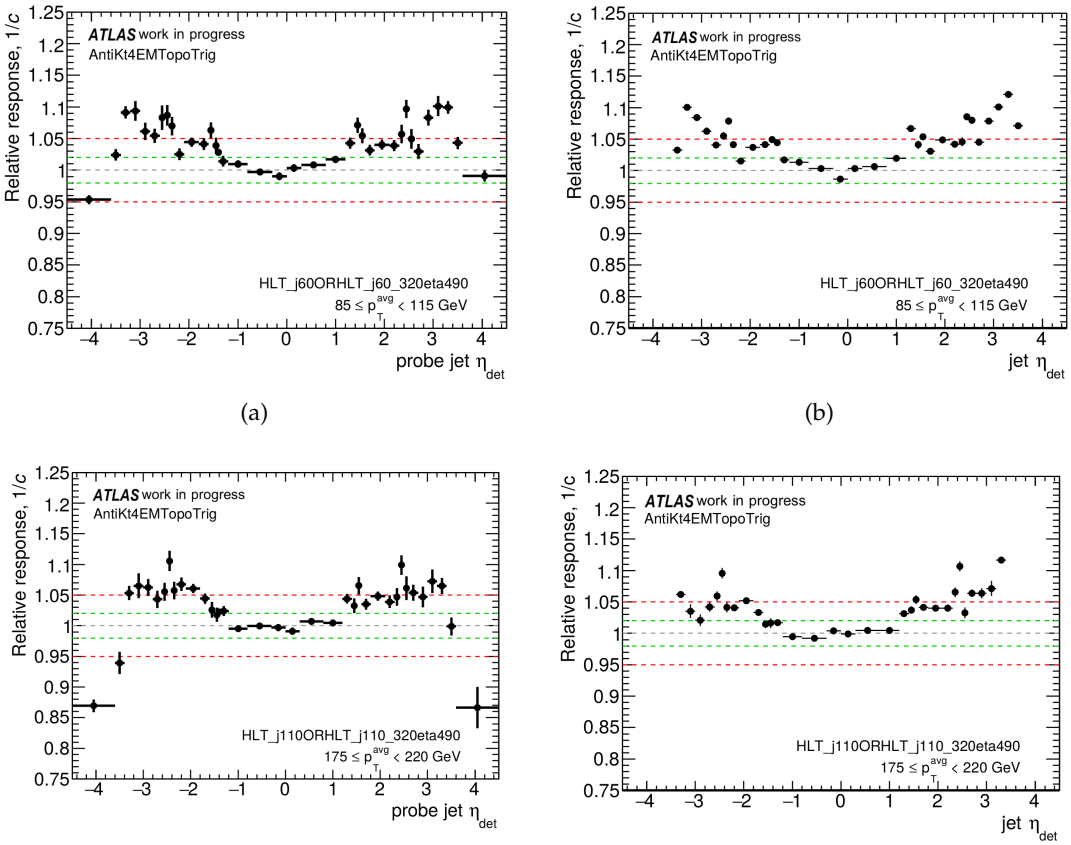


Figure 25: Comparison of standard (a,c) and matrix method (b,d).

### 5.2.3 *Comparison of data with MC*

In this section, a data-driven in-situ calibration is compared to the MC simulations. Four $p_T$ regions are used: $85 \leqslant p_T^{avg} < 115$ GeV, $175 \leqslant p_T^{avg} < 220$ GeV, $330 \leqslant p_T^{avg} < 400$ GeV, and $525 \leqslant p_T^{avg} < 760$ GeV. Regions with $p_T > 300$ GeV represent mid to high $p_T$ jets.

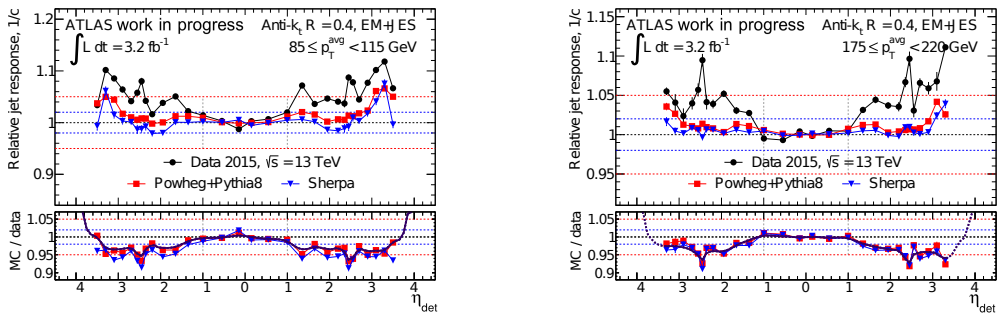

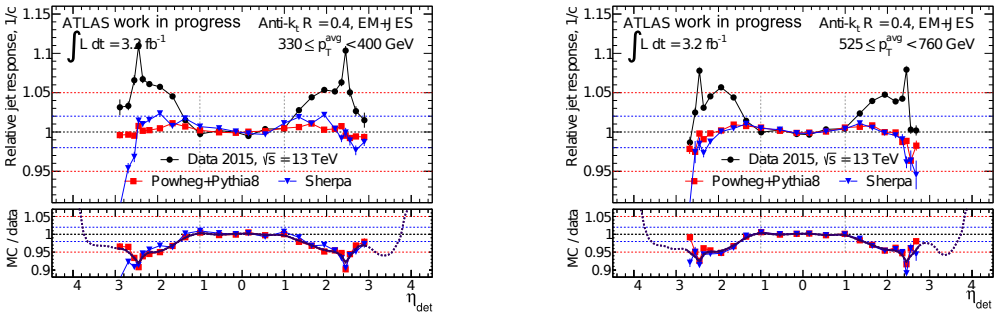


(c) (d)

Figure 24: Comparison between data and MC for different $p_T$ regions.

As opposed to the previous study in [30], MC simulation *cannot* reproduce jet responses as seen in data. Even though it has the same trend, the magnitude of the detector effect is evident. Two different MC simulations were used as a comparison, Powheg+Pythia8 and Sherpa. Both are needed to derive nominal and systematic uncertainties for the final jet energy scale uncertainties. The differences between two MC generator arise because of the different parton showering model being used.

### 5.2.4 *Trigger and offline jet comparison*

A comparison between the offline and online jet with the in-situ calibration are presented in the same $p_T$ regions as in the previous section. In Figure 23, the HLT jets agree well with its offline counterpart. The largest discrepancy observed is 4% in the transitional region ($\eta$=1.4) between barrel and forward regions for low-$p_T$ jets. There are some differences in more forward regions as well, but it would not have any effect in the TLA because a cut in $\eta$=2.2 will be applied. This effect is considerably smaller in the higher $p_T$ region since high-$p_T$ jets tend to fall in the more central region.

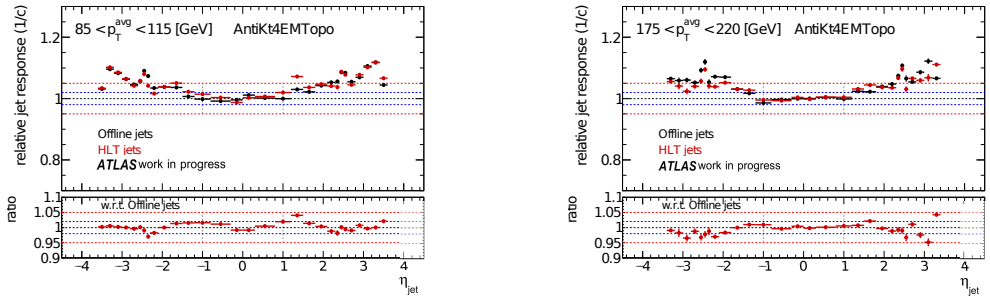


(a) (b)

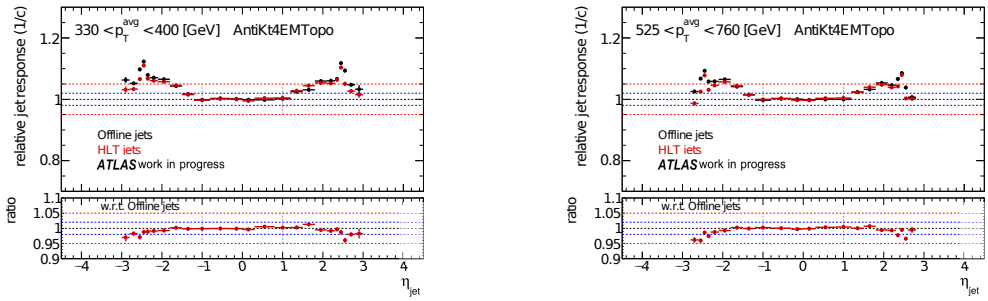


(c) (d)

Figure 23: Comparison between HLT and offline jets for differnet $p_T$ regions.

## 5.3 VALIDATION WITH MULTIJET EVENTS

The multijet balance technique is used to validate the calibration process. It is performed by taking the ratio between offline and HLT (online) jets. A value close to unity means the online jet calibration is able to perform well with regards to the offline one. Figure 24 shows the HLT jets has same trends with the offline jets. The difference is

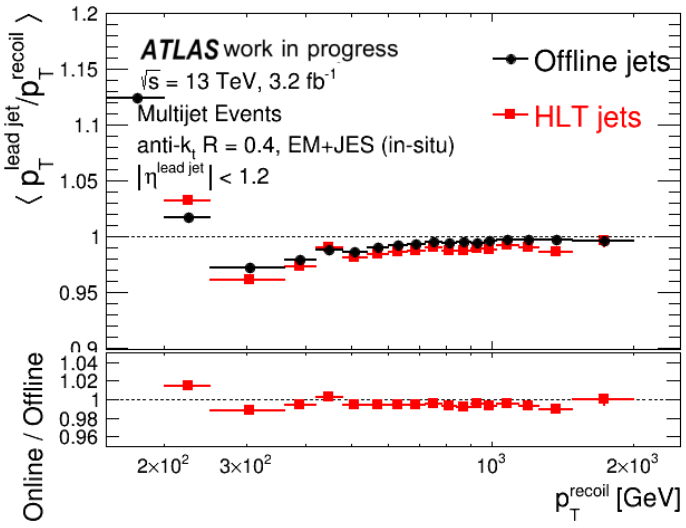


Figure 24: Multi-jet balance validation to EM+JES scale calibration

expected at around 2 percent across the whole range. Spikes in the low-$p_T$ region are due to the non-efficient trigger combined with the low-statistics data.

# 6

# SUMMARY

The $\eta$ inter-calibration for HLT jets was studied and derived by using both central reference and matrix method. Matrix method proved to be a better method because it has more statistics. A detector-dependence effect, especially in the problematic region at $|\eta|$=1.4,2.4 that cannot be corrected by Monte Carlo simulation was addressed. The calibration coefficient was calculated and the effect is almost negligible in the barrel region ($\eta$<1.0). It varied between 3-5% across the more forward region except in the transitional region between barrel and forward regions, which could reach 10%. This discrepancy also gives strong motivation for exploring more data-driven calibrations, especially for HLT jets. For the time being, it is considered sufficient to apply offline inter-calibration factors to exploit the central derivation of the uncertainties, and let the last step of the online-offline calibration takes care of the remaining differences.

Another important note is that HLT and offline jets agree pretty well after the calibration. With only a limited amount of information, this calibration only leads to discrepancies at around 2% across the detector range. The benefit of this finding is twofold. First, it acts as a strong evidence that HLT jets could be used in the analysis because they have a good agreement with the offline jets. Second, it opens a new possibility of using online and offline jet calibration interchangeably. The TLA has proved this in [27] that offline correction could be applied to HLT jets. This decision by the TLA team is understandable because offline jets are much more understood and well calibrated, at least in 2015 run.

Validation of this calibration method is done using multijet balance method. Other than the spike in low $p_T$ because of trigger turn-on, offline and online jets agree with 2-3% discrepancies.

On a further note beyond this thesis, the study on the jet response difference between data and MC in the forward region will also benefit from further studies. This could also help to simulate detector effects better. In 2016 run, tracking information will be added to online jets, which will bring further possibilities for calibrating HLT jets.

# APPENDIX

## A.1 COMPARISON OF DATA WITH MC

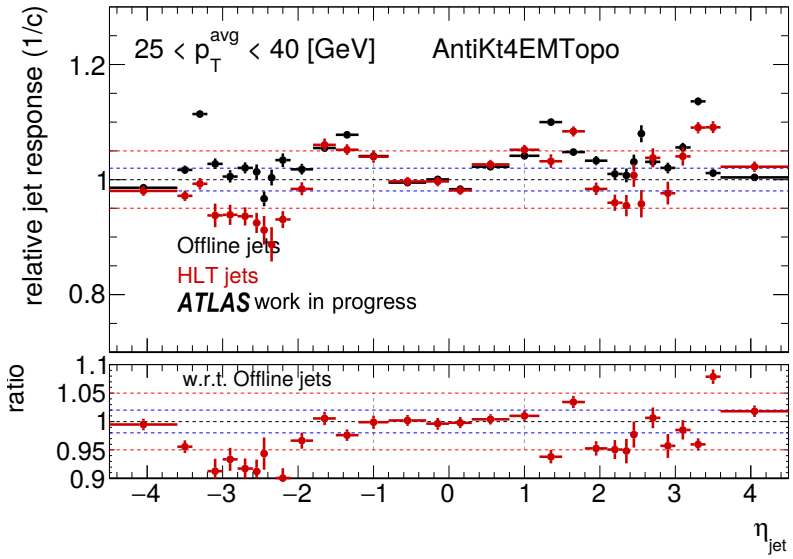


(a) MC-data η-intercalibration comparison binned in $25<p_T<40$.

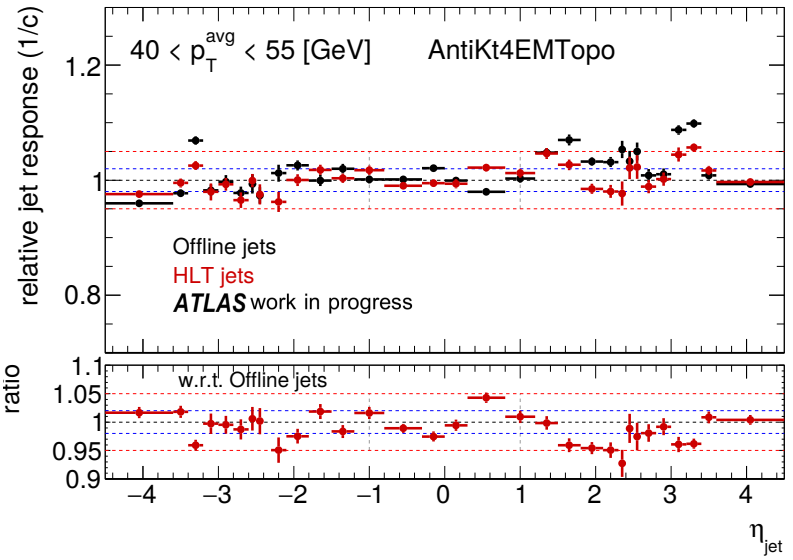


(b) MC-data η-intercalibration comparison binned in $40<p_T<55$.

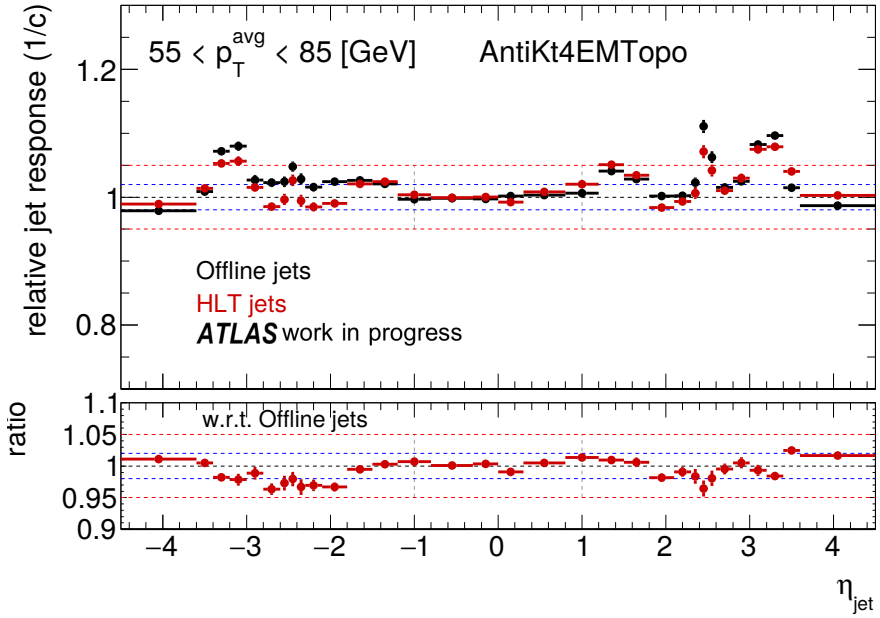


(c) MC-data η-intercalibration comparison binned in $55<p_T<85$.

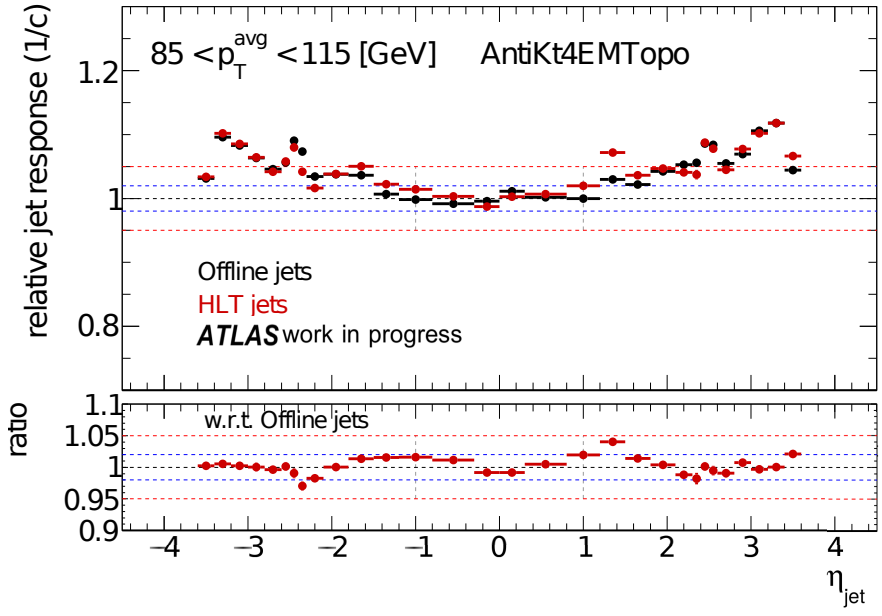


(d) MC-data η-intercalibration comparison binned in $85<p_T<115$.

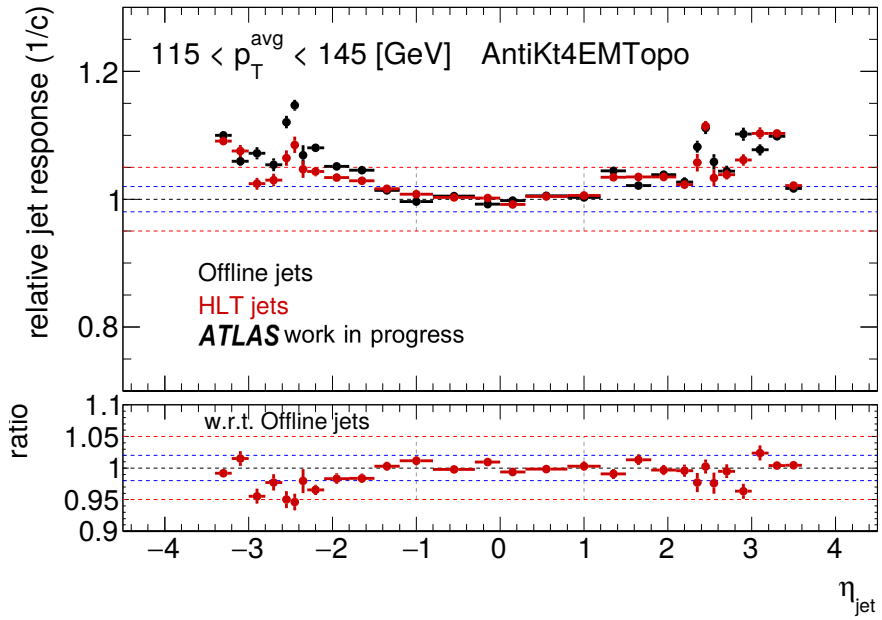


(e) MC-data η-intercalibration comparison binned in $115<p_T<145$.

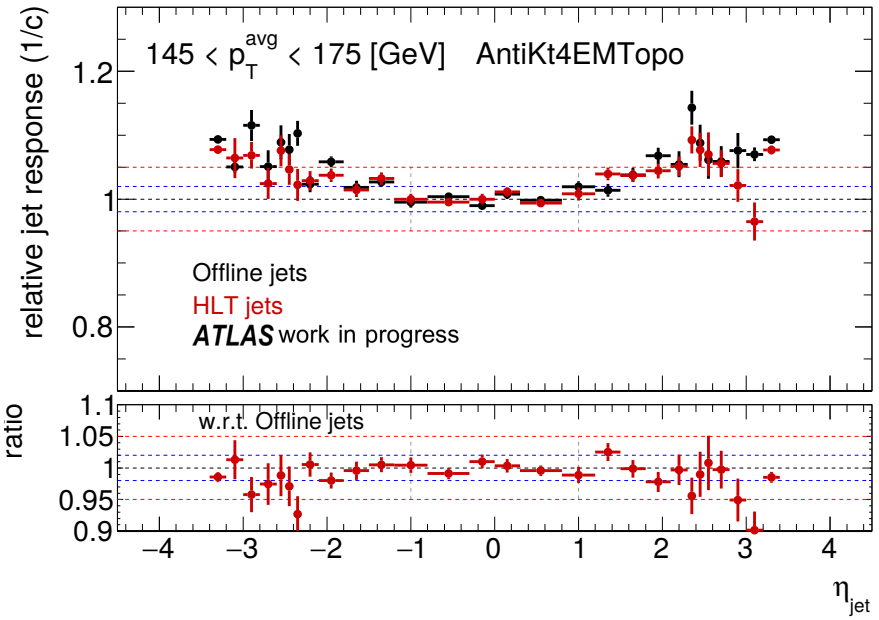


(f) MC-data η-intercalibration comparison binned in $145<p_T<175$.

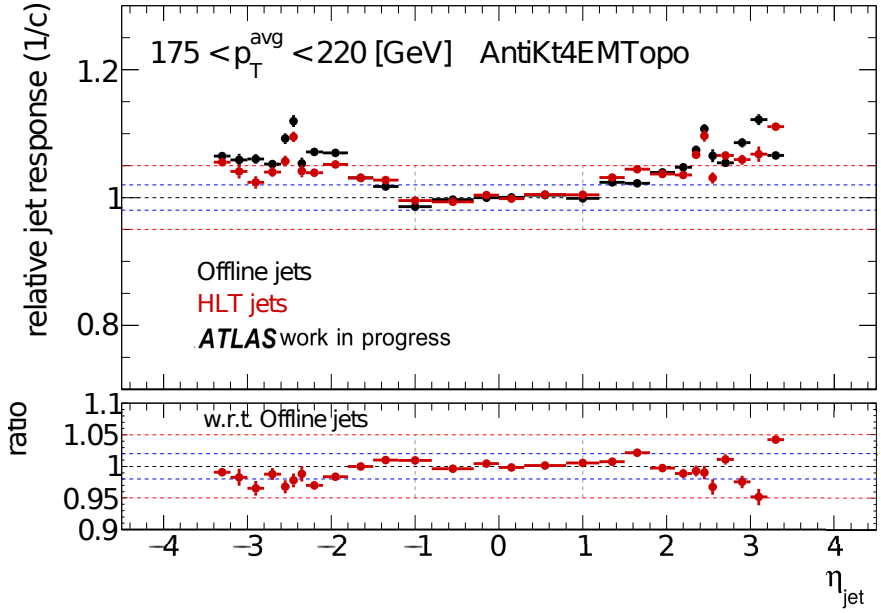


(g) MC-data η-intercalibration comparison binned in $175<p_T<220$.

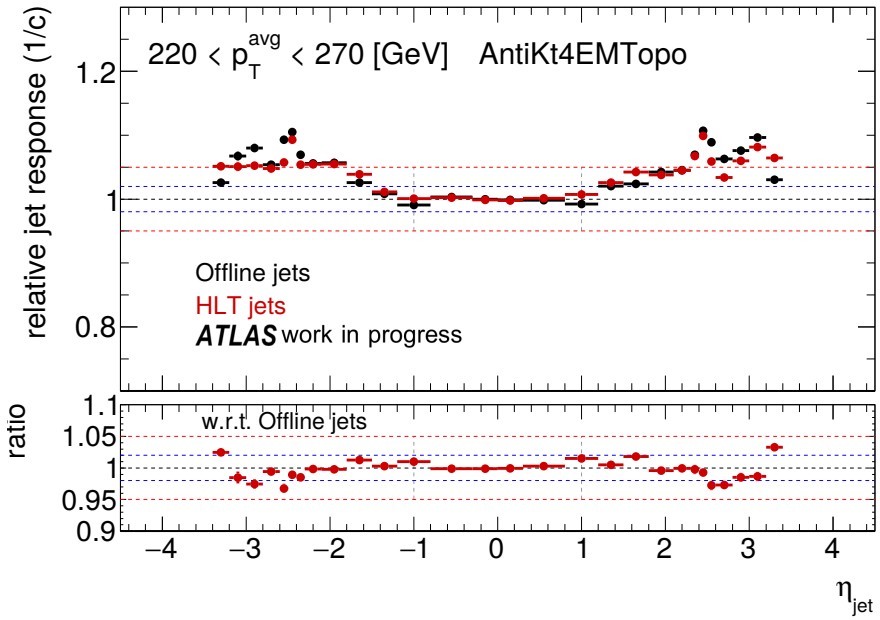


(h) MC-data η-intercalibration comparison binned in $220<p_T<270$.

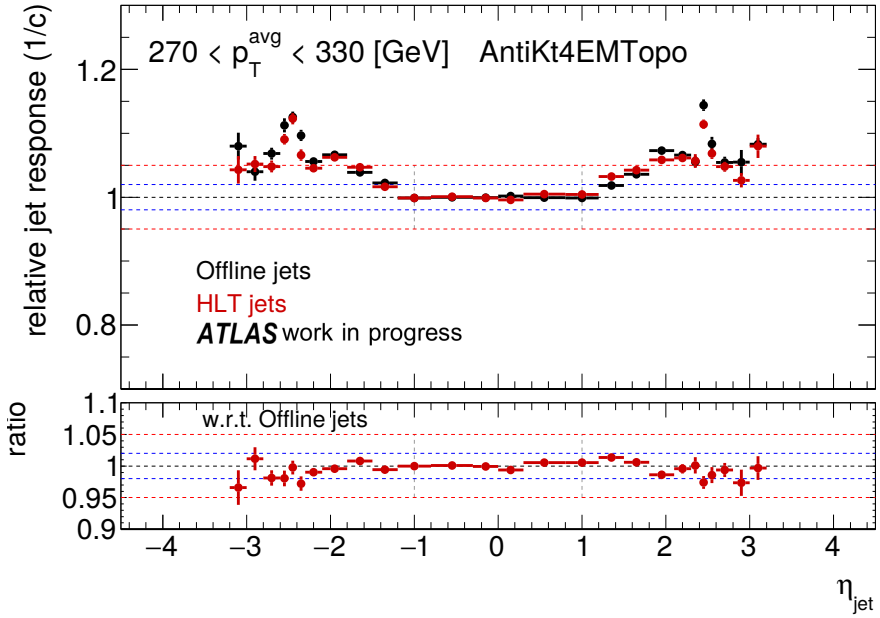


(i) MC-data η-intercalibration comparison binned in $270<p_T<330$.

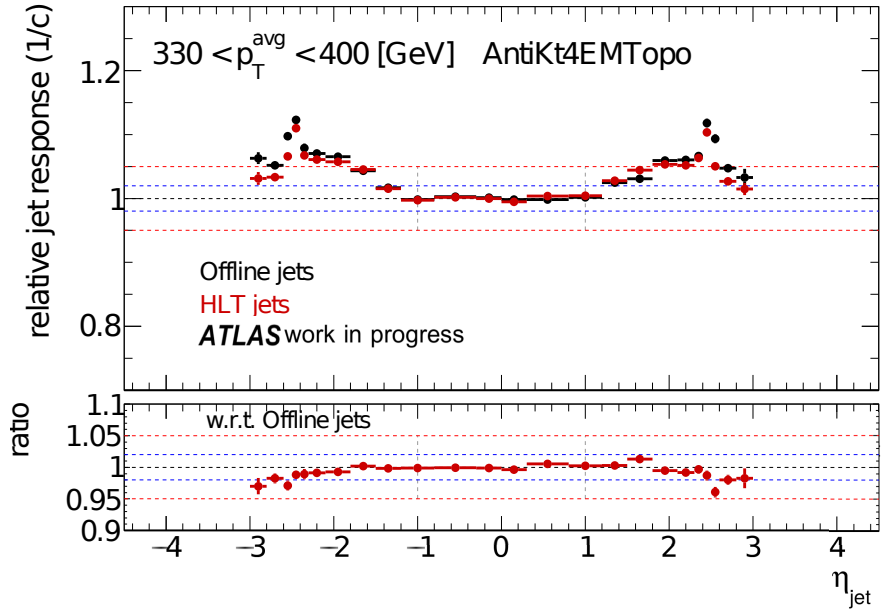


(j) MC-data η-intercalibration comparison binned in $330<p_T<400$.

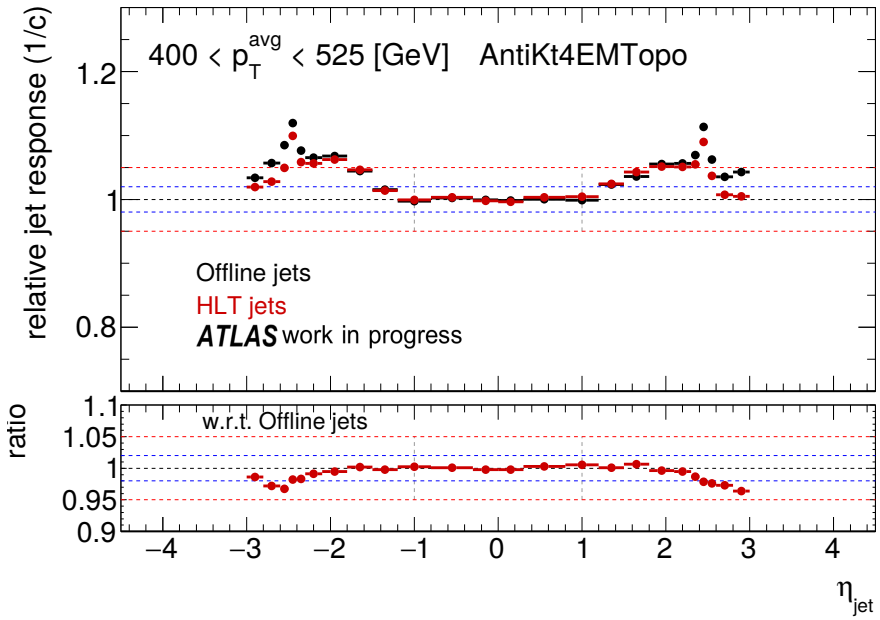


(k) MC-data η-intercalibration comparison binned in $400<p_T<525$.

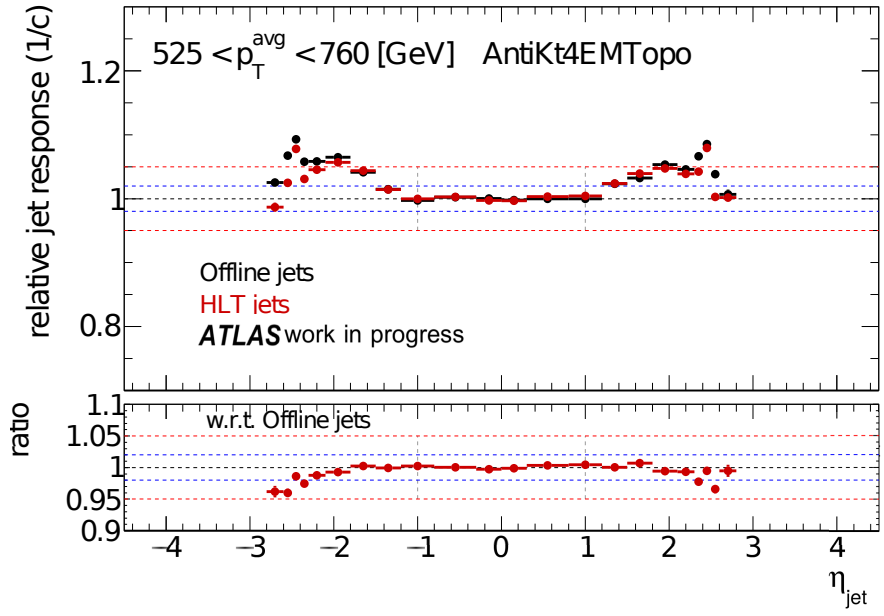


(l) MC-data η-intercalibration comparison binned in $525<p_T<760$.

Figure -5: Comparison of eta intercalibration applied in data and Monte Carlo for different $p_T$ ranges.

## A.2 TRIGGER AND OFFLINE JET COMPARISON

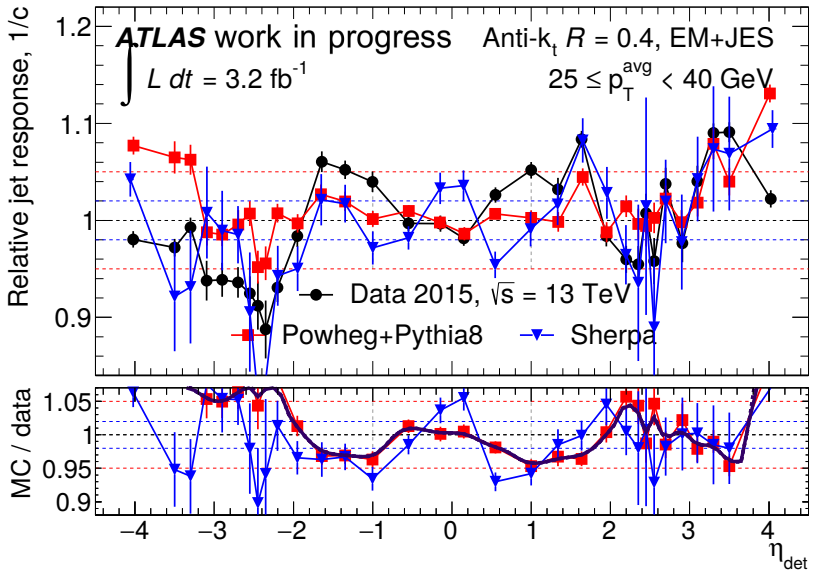


(a) HLT-offline jet η-intercalibration comparison binned in $25<p_T<40$.

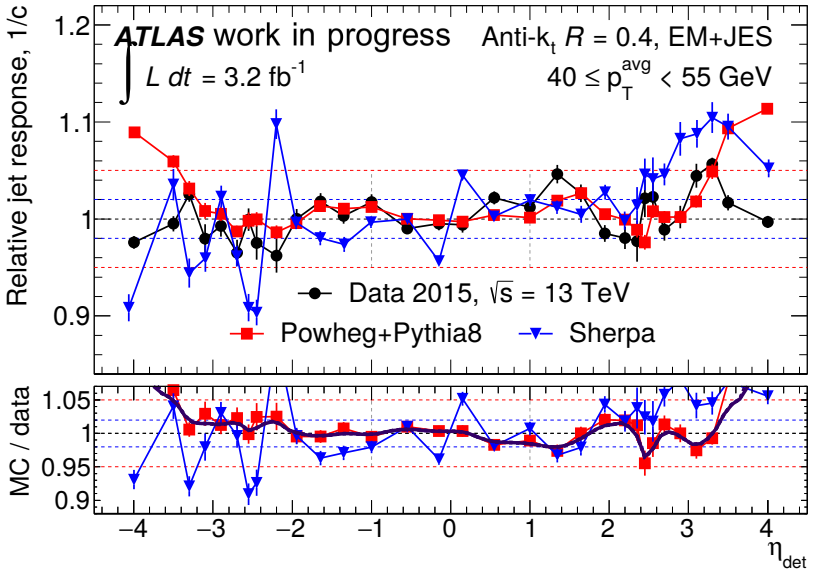


(b) HLT-offline jet η-intercalibration comparison binned in $40<p_T<55$.

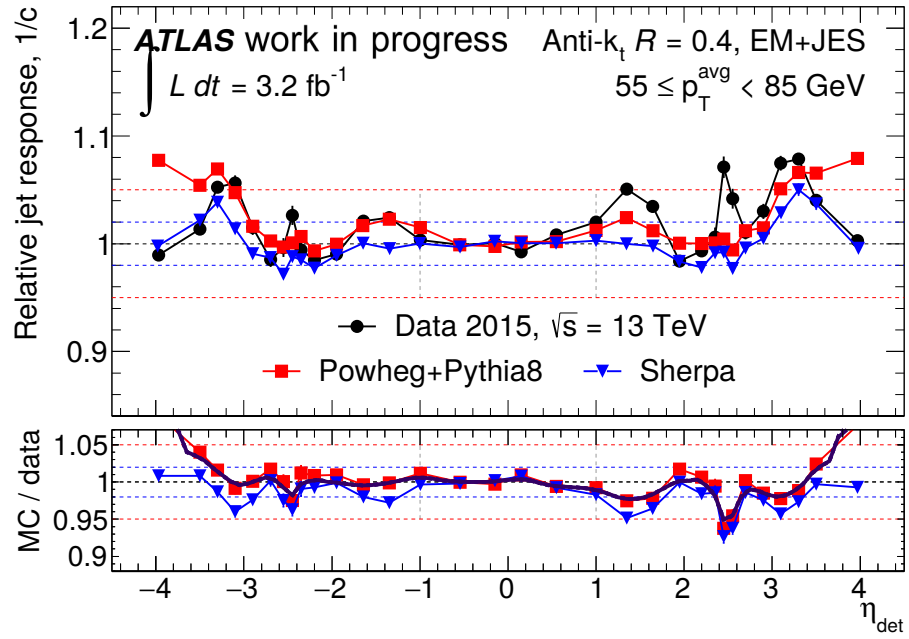


(c) HLT-offline jet η-intercalibration comparison binned in $55<p_T<85$.

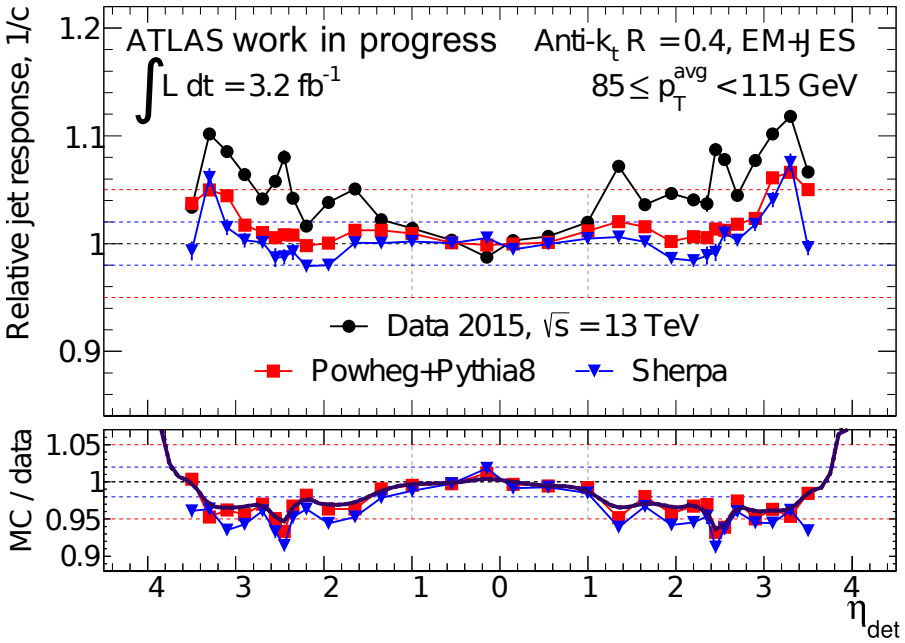


(d) HLT-offline jet η-intercalibration comparison binned in $85<p_T<115$.

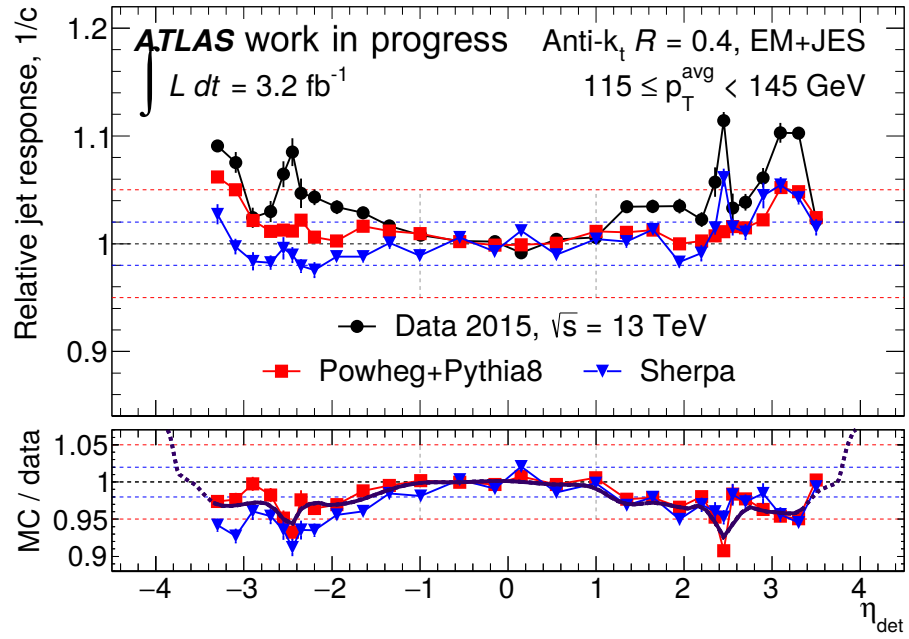


(e) HLT-offline jet η-intercalibration comparison binned in $115<p_T<145$.

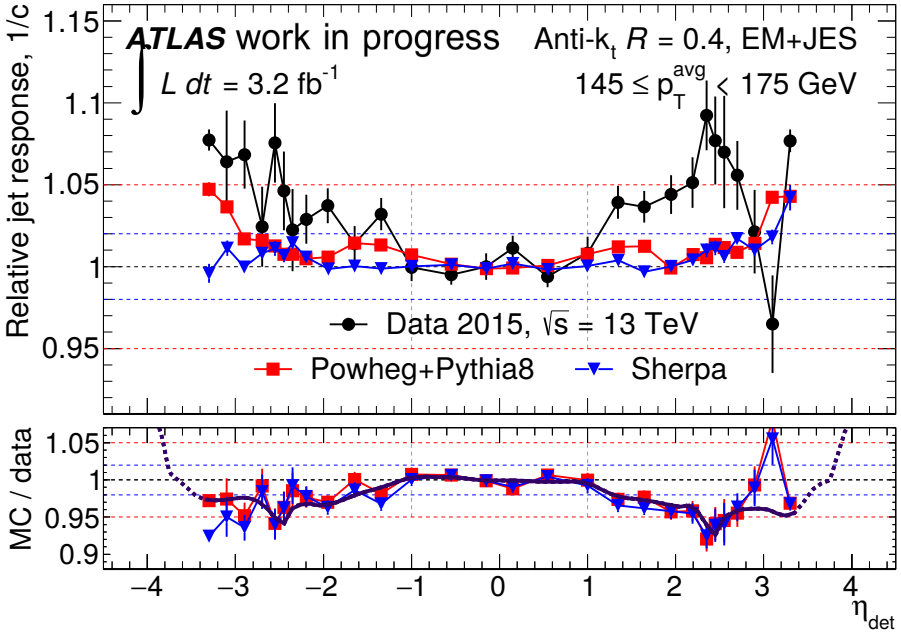


(f) HLT-offline jet η-intercalibration comparison binned in $145<p_T<175$.

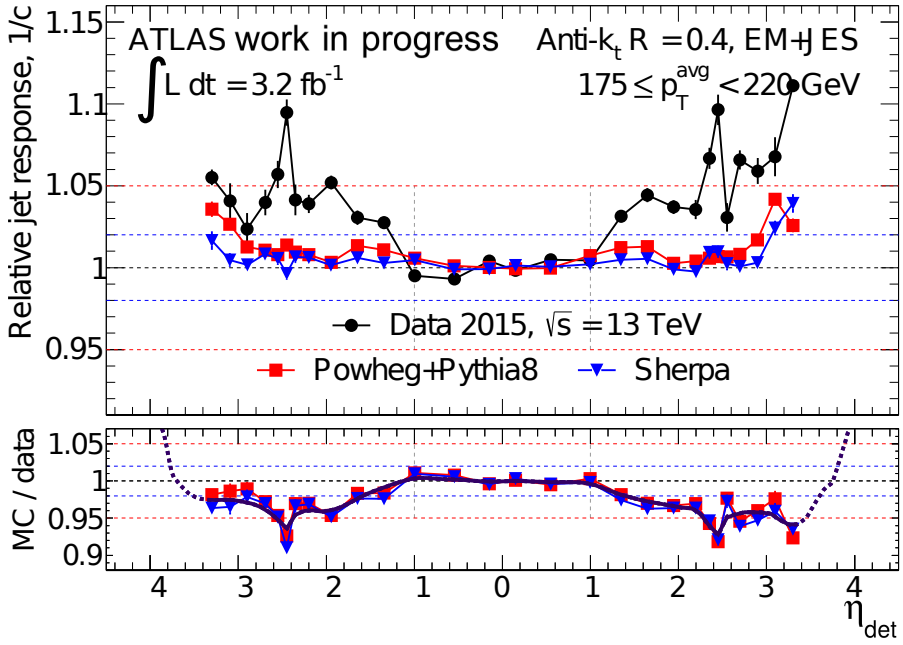


(g) HLT-offline jet η-intercalibration comparison binned in $175<p_T<220$.

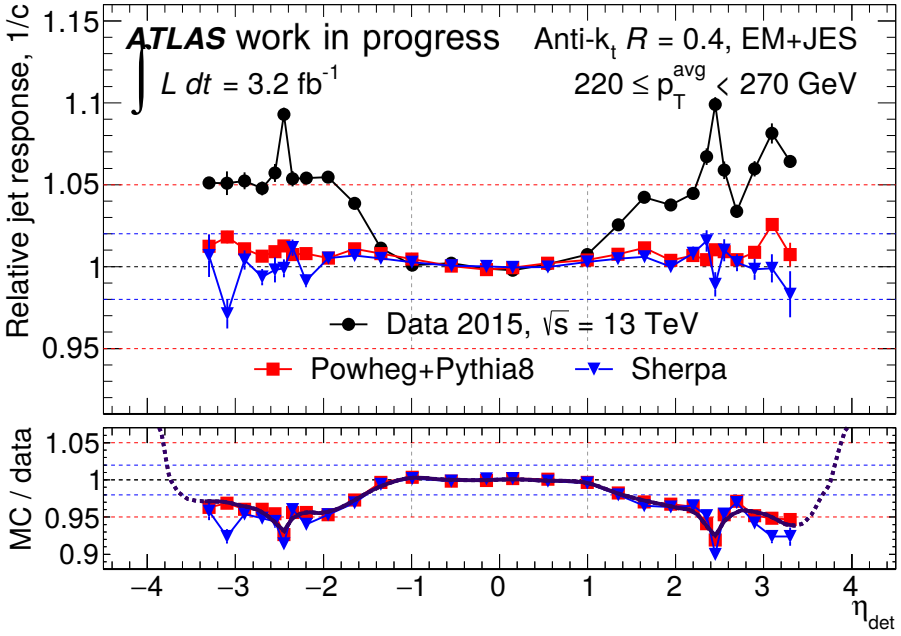


(h) HLT-offline jet η-intercalibration comparison binned in $220<p_T<270$.

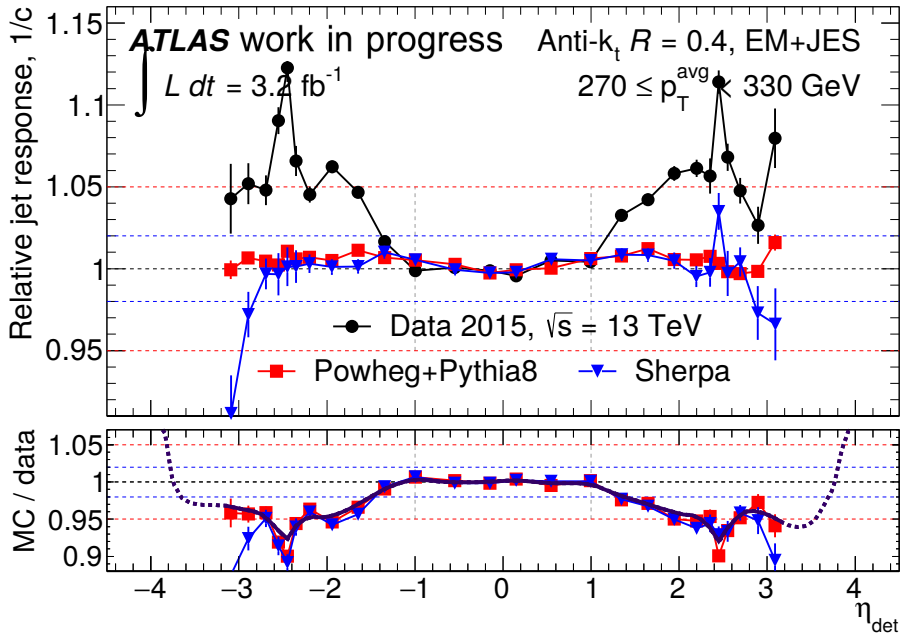


(i) HLT-offline jet η-intercalibration comparison binned in $270<p_T<330$.

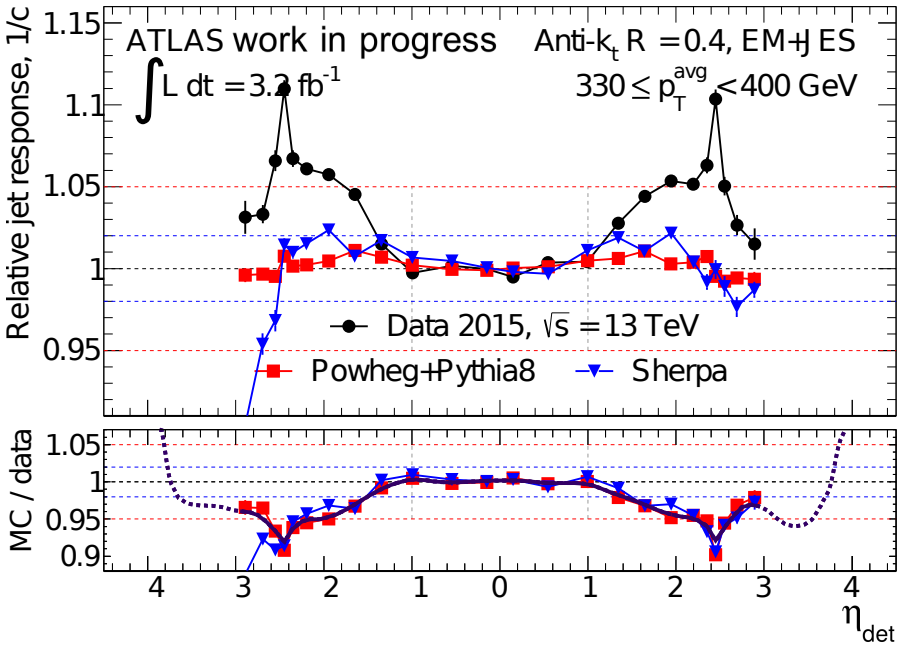


(j) HLT-offline jet η-intercalibration comparison binned in $330<p_T<400$.

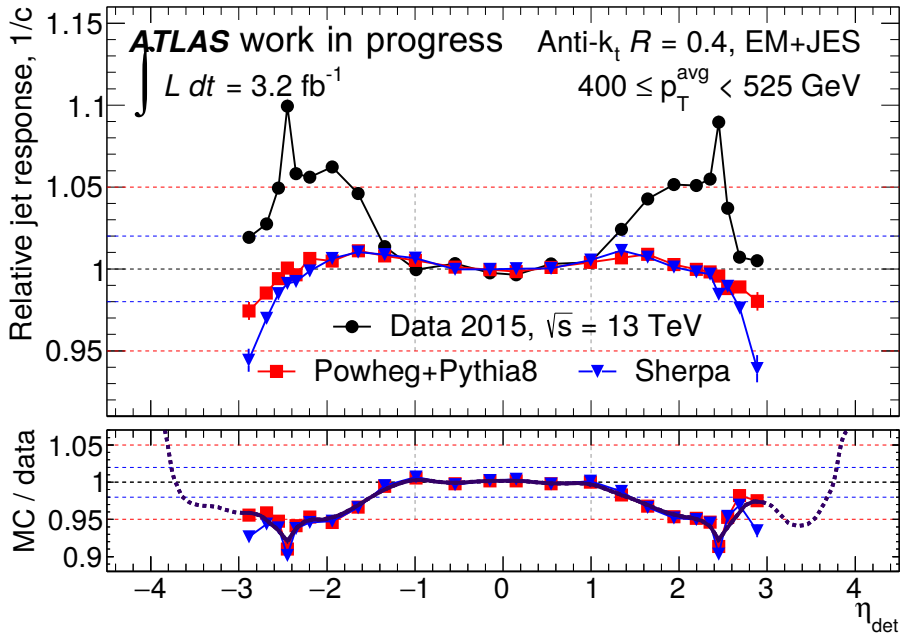


(k) HLT-offline jet η-intercalibration comparison binned in $400<p_T<525$.

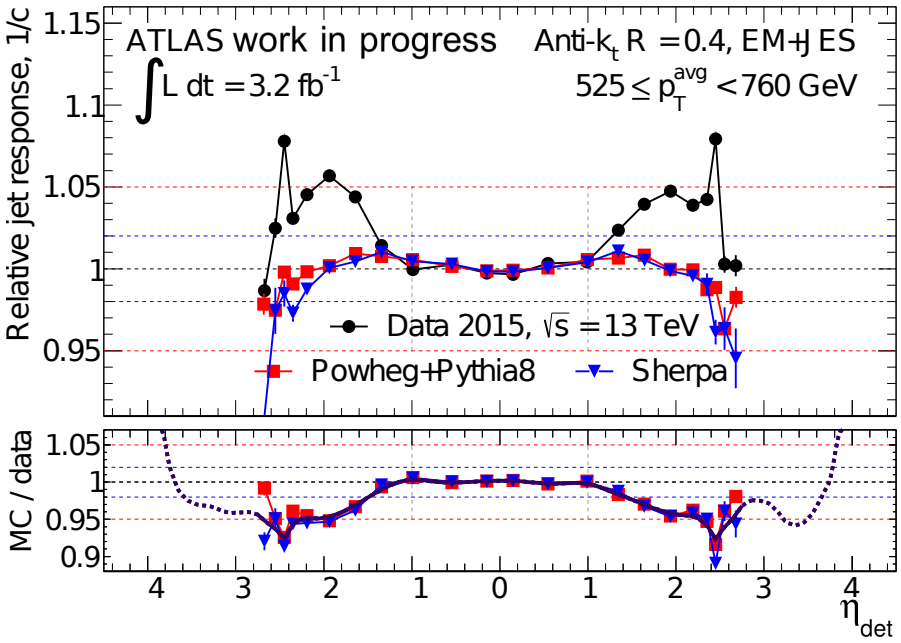


(l) HLT-offline jet η-intercalibration comparison binned in $525<p_T<760$.

Figure -10: Comparison of eta intercalibration between trigger and offline jets for different $p_T$ ranges.

# BIBLIOGRAPHY


[1] A. Zee RICHARD P. FEYNMAN. *QED: The Strange Theory of Light and Matter*. STU - Student edition. Princeton University Press, 1985. ISBN: 0691125759. URL: http://www.jstor.org/stable/j.ctt2jc8td.

[2] Mikael Chala, Felix Kahlhoefer, Matthew McCullough, Germano Nardini, and Kai Schmidt-Hoberg. "Constraining Dark Sectors with Monojets and Dijets." In: *JHEP* 07 (2015), p. 089. DOI: 10.1007/JHEP07(2015)089. arXiv: 1503.05916 [hep-ph].

[3] Daniel Abercrombie et al. "Dark Matter Benchmark Models for Early LHC Run-2 Searches: Report of the ATLAS/CMS Dark Matter Forum." In: (2015). Ed. by Antonio Boveia, Caterina Doglioni, Steven Lowette, Sarah Malik, and Stephen Mrenna. arXiv: 1507.00966 [hep-ex].

[4] Georges Aad et al. "Search for new phenomena in the dijet mass distribution using $p-p$ collision data at $\sqrt{s} = 8$ TeV with the ATLAS detector." In: *Phys. Rev.* D91.5 (2015), p. 052007. DOI: 10.1103/PhysRevD.91.052007. arXiv: 1407.1376 [hep-ex].

[5] Caterina Doglioni, Herjuno Rah Nindhito, Tim Martin, Stewart Martin-Haugh, Steven Schramm, Andrew Pilkington, Catrin Bernius, and Antonio Boveia. *Performance plots of data scouting trigger rates on 13 TeV data*. Tech. rep. ATL-COM-DAQ-2015-190. We would like to make these plots public by next Thursday so that they can be shown at a seminar and at a subsequent workshop. Geneva: CERN, Oct. 2015. URL: https://cds.cern.ch/record/2062992.

[6] Antonio Boveia et al. *Eta intercalibration plot from jet trigger group for LPCC poster: Eta intercalibration plots for trigger jets, corresponding to offline jet intercalibration plots: https://cds.cern.ch/record/2132457/files/ATL-COM-PHYS-2016-138.pdf*. Tech. rep. ATL-COM-DAQ-2016-017. Prepared for LPCC poster session of March 2nd. Geneva: CERN, Feb. 2016. URL: https://cds.cern.ch/record/2133173.

[7] Antonio Boveia et al. *Jet Data Scouting plots for approval*. Tech. rep. ATL-COM-DAQ-2016-012. We would like to present those plots at a seminar on the week of Monday 22nd of February and at the LPCC poster session on March 2nd. Geneva: CERN, Oct. 2016. URL: https://cds.cern.ch/record/2130838.

[8] G. P. S. Occhialini and C. F. Powell. "Nuclear Disintegrations Produced by Slow Charged Particles of Small Mass." In: *Nature* 159 (Feb. 1947), pp. 186–190. DOI: 10.1038/159186a0. URL: %5Curl%7Bhttp://adsabs.harvard.edu/abs/1947Natur.159..186O%7D.

[9] K. A. Olive et al. "Review of Particle Physics." In: *Chin. Phys.* C38 (2014), p. 090001. DOI: 10.1088/1674-1137/38/9/090001.

[10] ATLAS collaboration. *A high-mass dijet event*. https://twiki.cern.ch/twiki/bin/view/AtlasPublic/EventDisplayRun2Collisions. 2015 (accessed April 1, 2016).

[11] Nuno Anjos. *The ATLAS Jet Trigger for Run2*. http://indico.ifae.es/getFile.py/access?contribId=1&resId=0&materialId=slides&confId=126. 2010.

[12] Andy Buckley et al. "General-purpose event generators for LHC physics." In: *Phys. Rept.* 504 (2011), pp. 145–233. DOI: 10.1016/j.physrep.2011.03.005. arXiv: 1101.2599 [hep-ph].

[13] Lars Bergstrom. "Dark Matter Evidence, Particle Physics Candidates and Detection Methods." In: *Annalen Phys.* 524 (2012), pp. 479–496. DOI: 10.1002/andp.201200116. arXiv: 1205.4882 [astro-ph.HE].

[14] Andrew Askew, Sushil Chauhan, Bjorn Penning, William Shepherd, and Mani Tripathi. "Searching for Dark Matter at Hadron Colliders." In: *Int. J. Mod. Phys.* A29 (2014), p. 1430041. DOI: 10.1142/S0217751X14300415. arXiv: 1406.5662 [hep-ph].

[15] Bogdan A. Dobrescu and Felix Yu. "Coupling-mass mapping of dijet peak searches." In: *Phys. Rev.* D88.3 (2013). [Erratum: Phys. Rev.D90,no.7,079901(2014)], p. 035021. DOI: 10.1103/PhysRevD.88.035021, 10.1103/PhysRevD.90.079901. arXiv: 1306.2629 [hep-ph].

[16] Cinzia De Melis. "The CERN accelerator complex." In: (Jan. 2016). General Photo. URL: https://cds.cern.ch/record/2119882.

[17] Jorg Wenninger for the LHC team. "LHC Report: 1,033 bunches per beam and counting." In: BUL-NA-2015-201. 39/2015 (Sept. 2015), p. 3. URL: https://cds.cern.ch/record/2053142.

[18] ATLAS collaboration. *Total Integrated Luminosity and Data Quality in 2015*. https://twiki.cern.ch/twiki/bin/view/AtlasPublic/LuminosityPublicResultsRun2. 2015 (accessed April 5, 2016).

[19] G Aad et al. "The ATLAS Experiment at the CERN Large Hadron Collider." In: *J. Instrum.* 3 (2008). Also published by CERN Geneva in 2010, So8003. 437 p. URL: https://cds.cern.ch/record/1129811.

[20] P. Puzo. "ATLAS calorimetry." In: *Nucl. Instrum. Meth.* A494 (2002), pp. 340–345. DOI: 10.1016/S0168-9002(02)01490-0.

[21] Jeremiah Jet Goodson and Robert McCarthy. "Search for Supersymmetry in States with Large Missing Transverse Momentum and Three Leptons including a Z-Boson." Presented 17 Apr 2012. PhD thesis. Stony Brook U., May 2012. URL: https://cds.cern.ch/record/1449722.

[22] Stephen D. Ellis and Davison E. Soper. "Successive combination jet algorithm for hadron collisions." In: *Phys. Rev.* D48 (1993), pp. 3160–3166. DOI: 10.1103/PhysRevD.48.3160. arXiv: hep-ph/9305266 [hep-ph].

[23] Yuri L. Dokshitzer, G. D. Leder, S. Moretti, and B. R. Webber. "Better jet clustering algorithms." In: *JHEP* 08 (1997), p. 001. DOI: 10.1088/1126-6708/1997/08/001. arXiv: hep-ph/9707323 [hep-ph].

[24] Matteo Cacciari, Gavin P. Salam, and Gregory Soyez. "The Anti-k(t) jet clustering algorithm." In: *JHEP* 04 (2008), p. 063. DOI: 10.1088/1126-6708/2008/04/063. arXiv: 0802.1189 [hep-ph].

[25] *Calibration of ATLAS* b*-tagging algorithms in dense jet environments*. Tech. rep. ATLAS-CONF-2016-001. Geneva: CERN, Feb. 2016. URL: http://cds.cern.ch/record/2127958.

[26] Nuno Anjos et al. *The ATLAS Jet Trigger for Initial LHC Run II*. Tech. rep. ATL-COM-DAQ-2015-164. Geneva: CERN, Sept. 2015. URL: https://cds.cern.ch/record/2055279.

[27] Ricardo Abreu et al. *Search for low-mass dijet resonances with Trigger-Level Analysis*. Tech. rep. ATL-COM-PHYS-2016-049. Geneva: CERN, Jan. 2016. URL: https://cds.cern.ch/record/2125945.

[28] Steven Schramm. *Jet trigger calibration discussion*. https://indico.cern.ch/event/472326/contributions/1148843/attachments/1242904/1828867/StevenSchramm-Calibration.pdf. 2016 (accessed March 14, 2016).

[29] *In-situ pseudo-rapidity inter-calibration to evaluate jet energy scale uncertainty and calorimeter performance in the forward region*. Tech. rep. ATLAS-CONF-2010-055. Geneva: CERN, July 2010. URL: http://cds.cern.ch/record/1281312.

[30] *In situ jet pseudorapidity intercalibration of the ATLAS detector using dijet events in sqrts=7 TeV proton-proton 2011 data*. Tech. rep. ATLAS-CONF-2012-124. Geneva: CERN, Aug. 2012. URL: http://cds.cern.ch/record/1474490.

[31] *Probing the jet energy measurement at the TeV-scale using the multi-jet balance technique in proton-proton collisions at sqrt(s) =7 TeV*. Tech. rep. ATLAS-CONF-2011-029. Geneva: CERN, Mar. 2011. URL: http://cds.cern.ch/record/1337076.

[32] LPSC Grenoble. *ATLAS Metadata Interface*. https://ami.in2p3.fr/. 2016 (accessed April 13, 2016).

[33] *COMA Period Documentation Menu*. https://atlas-tagservices.cern.ch/tagservices/RunBrowser/index.html. 2016 (accessed April 13, 2016).

[34] Paolo Nason and Bryan Webber. "Next-to-Leading-Order Event Generators." In: *Ann. Rev. Nucl. Part. Sci.* 62 (2012), pp. 187–213. DOI: 10.1146/annurev-nucl-102711-094928. arXiv: 1202.1251 [hep-ph].

[35] Torbjorn Sjostrand, Stephen Mrenna, and Peter Z. Skands. "A Brief Introduction to PYTHIA 8.1." In: *Comput. Phys. Commun.* 178 (2008), pp. 852–867. DOI: 10.1016/j.cpc.2008.01.036. arXiv: 0710.3820 [hep-ph].

[36] *ATLAS Run 1 Pythia8 tunes*. Tech. rep. ATL-PHYS-PUB-2014-021. Geneva: CERN, Nov. 2014. URL: https://cds.cern.ch/record/1966419.

[37] Sherpa Team. *The complete list of Sherpa's parameters*. http://sherpa.hepforge.org/doc/Sherpa.html. 2015 (accessed April 10, 2016).

[38] Robert Hofstadter and Robert W. McAllister. "Electron Scattering from the Proton." In: *Phys. Rev.* 98 (1 Apr. 1955), pp. 217–218. DOI: 10.1103/PhysRev.98.217. URL: %5Curl%7Bhttp://link.aps.org/doi/10.1103/PhysRev.98.217%7D.

[39] E. Dudas, Y. Mambrini, S. Pokorski, and A. Romagnoni. "(In)visible Z-prime and dark matter." In: *JHEP* 08 (2009), p. 014. DOI: 10.1088/1126-6708/2009/08/014. arXiv: 0904.1745 [hep-ph].

[40] Qian-Fei Xiang, Xiao-Jun Bi, Peng-Fei Yin, and Zhao-Huan Yu. "Searches for dark matter signals in simplified models at future hadron colliders." In: *Phys. Rev.* D91 (2015), p. 095020. DOI: 10.1103/PhysRevD.91.095020. arXiv: 1503.02931 [hep-ph].

[41] Ricardo Lince Amaral Farto Abreu et al. *Data Scouting in ATLAS: Trigger, Tiero and Analysis*. Tech. rep. ATL-COM-GEN-2014-010. Geneva: CERN, Oct. 2014. URL: https://cds.cern.ch/record/1957173.

[42] W.J. Stirling. personal communication. 2015.

[43] ATLAS Collaboration. *The main ATLAS trigger menu for 2015 pp collisions at 13 TeV*. https://twiki.cern.ch/twiki/bin/view/AtlasPublic/TriggerOperationPublicResults. 2015.

[44] Ricardo Abreu et al. *Search for low-mass dijet resonances with Trigger-Level Analysis*. Tech. rep. ATL-COM-PHYS-2016-049. Geneva: CERN, Jan. 2016. URL: https://cds.cern.ch/record/2125945.

[45] *Jet global sequential corrections with the ATLAS detector in proton-proton collisions at sqrt(s) = 8 TeV*. Tech. rep. ATLAS-CONF-2015-002. Geneva: CERN, Mar. 2015. URL: https://cds.cern.ch/record/2001682.

[46] John Alison et al. *Search for new light resonances decaying to jet pairs in association with a photon in proton-proton collisions at* $\sqrt{s} = 13$ *TeV with the ATLAS detector*. Tech. rep. ATLAS-COM-CONF-2016-035. Geneva: CERN, May 2016. URL: https://cds.cern.ch/record/2155347.